

A spatial causal analysis of wildland fire-contributed $PM_{2.5}$ using numerical model output

Alexandra E Larsen^{1,2}, Shu Yang¹, Brian J Reich¹ and Ana G Rappold³

March 16, 2020

Abstract

Wildland fire smoke contains hazardous levels of fine particulate matter ($PM_{2.5}$), a pollutant shown to adversely effect health. Estimating fire attributable $PM_{2.5}$ concentrations is key to quantifying the impact on air quality and subsequent health burden. This is a challenging problem since only total $PM_{2.5}$ is measured at monitoring stations and both fire-attributable $PM_{2.5}$ and $PM_{2.5}$ from all other sources are correlated in space and time. We propose a framework for estimating fire-contributed $PM_{2.5}$ and $PM_{2.5}$ from all other sources using a novel causal inference framework and bias-adjusted chemical model representations of $PM_{2.5}$ under counterfactual scenarios. The chemical model representation of $PM_{2.5}$ for this analysis is simulated using Community Multi-Scale Air Quality Modeling System (CMAQ), run with and without fire emissions across the contiguous U.S. for the 2008-2012 wildfire seasons. The CMAQ output is calibrated with observations from monitoring sites for the same spatial domain and time period. We use a Bayesian model that accounts for spatial variation to estimate the effect of wildland fires on $PM_{2.5}$ and state assumptions under which the estimate has a valid causal interpretation. Our results include estimates of absolute, relative and cumulative contributions of wildfire smoke to $PM_{2.5}$ for the contiguous U.S. Additionally, we compute the health burden associated with the $PM_{2.5}$ attributable to wildfire smoke.

¹Department of Statistics, North Carolina State University, Raleigh, NC

²Oak Ridge Institute for Science and Education at the United States Environmental Protection Agency, National Health and Environmental Effects Research Laboratory, Environmental Public Health Division, Research Triangle Park, NC

³United States Environmental Protection Agency, National Health and Environmental Effects Research Laboratory, Environmental Public Health Division, Research Triangle Park, NC. Disclaimer: This work does not necessarily represent EPA views or policy.

Key words: Interference; Spillover effect; Bayesian analysis; Downscaling.

1 Introduction

Wildfires have become a leading contributor to unhealthy air quality in many communities. Among the pollutants found in smoke, fine particulate matter (mixtures of particles smaller than $2.5 \mu m$ in diameter or $PM_{2.5}$), associated with a number of respiratory and cardiovascular outcomes, is of the largest public health concern (Dennekamp and Abramson, 2011; Rappold et al., 2011; Johnston et al., 2012; Dennekamp et al., 2015; Haikerwal et al., 2015, 2016; Wettstein et al., 2018). The objective of this study is to estimate wildland fire-attributable fraction of ambient $PM_{2.5}$ in order to quantify the related health burden. We introduce a potential outcomes framework to estimate the causal effect of wildland fires on ambient $PM_{2.5}$ in the presence of spatial correlation. The framework leverages numerical model simulations of air quality serving as biased representations of the potential outcomes. A Bayesian spatial downscaling model is used to learn the relationship between the spatially and temporally resolved numerical model output and the sparsely observed $PM_{2.5}$ from air quality monitors, and to provide unbiased estimates of counterfactual outcomes, quantification of uncertainty, and predictions that are both spatially and temporally resolved.

To quantify the magnitude of the health burden attributable to the smoke from fire events, we need to distinguish the $PM_{2.5}$ composition mixture attributable to fire from the $PM_{2.5}$ mixture due to all other sources. Total ambient $PM_{2.5}$ concentrations are recorded at the monitoring sites across the country, however, these observations do not provide insight into the potential composition of particles that would have formed had there been no wildfires. The mixture of particles measured on any given day depends on multiple sources of emissions and conditions of combustion by which particles were produced. Once released, particles and gases coalesce and interact with those already present in the atmosphere through non-additive chemical and physical processes. Formation of $PM_{2.5}$ is additionally confounded by external factors including fire weather conditions, vegetation,

burned areas and areas unable to burn again, as well as anthropogenic and other natural emissions (McKenzie et al., 2014; Stavros et al., 2014). Finally, in the presence of fire, non-fire emissions themselves can be altered through feedbacks. Together, these factors lead to complex dependencies of $\text{PM}_{2.5}$ concentrations across space and time.

To distinguish fire-contributed $\text{PM}_{2.5}$ from total ambient concentrations we utilize numerical model representations of air quality. The model simulates chemical reactions and transport of particle-mixtures in the atmosphere using deterministic representations of chemical processes under a set of input emissions and external forcings. By removing the forcing for wildfire emissions, these models produce air quality simulations from the counterfactual scenario, i.e. $\text{PM}_{2.5}$ composition that would have formed had there not been wildfires. In this study, we use the Community Multiscale Air Quality (CMAQ) numerical model to simulate air quality under observed and counterfactual forcings. The difference in $\text{PM}_{2.5}$ under CMAQ representations of air quality with and without wildfire emissions is considered to be a modeled representation of fire-contributed $\text{PM}_{2.5}$.

Numerical models have been used to simulate counterfactual environmental conditions in other contexts, most notably to investigate future unobserved or distant past climate trajectories (Allen and Stott, 2003; Hegerl and Zwiers, 2011; Nat, 2016; Katzfuss et al., 2017; Knutson et al., 2017). These studies, referred to as detection and attribution (D&A) studies, use global climate models to detect changes by varying an exogenous forcing while holding all else constant and to attribute the change to the specific forcings. These studies have been linked to causal counterfactual theory in Hannart et al. (2015) in which authors demonstrate the utility of deriving the probability of necessary and sufficient causality in formulating causal claims (Hannart et al., 2015). However, when outcomes are not directly observable (e.g. future or paleo climates), causal inference is limited due to lack of accounting for error and uncertainty (Hannart et al., 2015).

Even when the outcomes are observable, such as in the case of air quality, numerical models are subject to systematic bias arising from misspecification of inputs or processes governing model behavior. To calibrate the CMAQ $\text{PM}_{2.5}$ output in our study, we develop a Bayesian statistical downscaling method that relates data at a lower observed resolution

to a spatially resolved, higher resolution of CMAQ model and allows for spatial prediction at all locations. The calibration model is similar to the spatio-temporal downscaling method introduced by Berrocal et al. (2010) in that it uses spatially-varying coefficients to estimate the relationship between sparse observations and numeric model output where data is available (Gelfand et al., 2003; Schmidt and Gelfand, 2003; Gelfand et al., 2004; Berrocal et al., 2010). The method is computationally efficient and has high predictive performance relative to other downscaling methods (Cressie, 1993; Chilès and Delfiner, 2012; Fuentes and Raftery, 2005).

The second challenge to estimating wildfire attributed $PM_{2.5}$ concentrations within a causal inference paradigm is the spatial interference between the observed $PM_{2.5}$ at sites according to whether or not the site (observation unit) is impacted by wildfires (treatment). Indirect or spill-over effect across spatial locations violates the stable unit treatment value assumption (SUTVA), which is central to the potential outcomes framework for causal inference (Rubin, 1978). Estimating valid causal effects in the presence of interference has previously been addressed in the context of vaccines and infectious diseases (Hong and Raudenbush, 2006; Rosenbaum, 2007; Hudgens and Halloran, 2008; Tchetgen and VanderWeele, 2012).

Most commonly, interference has been addressed using the less stringent partial interference assumption, which assumes interference amongst units in the same group, but not between groups (Halloran and Struchiner, 1991; Sobel, 2006; Hudgens and Halloran, 2008). The problem of interference among units has also been addressed in estimating the causal effect of air pollution regulations on health burden (Zigler et al., 2012; Dominici et al., 2014; Zigler et al., 2017). Zigler et al. (2012) introduced the first application of spatial models to predict unobserved potential outcomes and develop causal effect estimate of air pollution regulations. To address the interference among units of observation, the authors rely on principal stratification and an assumption of partial interference. However, the correlation between units observed under opposite treatments is unidentifiable under their framework.

The main methodological contribution of this paper is to present a counterfactual

framework that utilizes bias-corrected numerical model output to produce valid causal inference in the presence of spatial spillover effects. The proposed framework estimates counterfactual outcomes for each day and location under two treatment regimes: the observed regime with wildfires and the unobservable regime without wildfires. We specify a Bayesian model to fuse the numerical model output with monitor data. We assume that conditional on numerical model output, observations in the areas not affected by smoke are representative of the counterfactual regime without wildfires. This allows us to bias-correct the CMAQ output from the counterfactual regimes with observed data, which has been the limitation of previous studies. Through numerical model simulations under both regimes we are able to estimate correlation between the units observed under different regimes. We clarify the assumptions required for the estimates to have a causal interpretation, and show if these assumptions hold then the proposed method accounts for spillover effects and that all model parameters are identified.

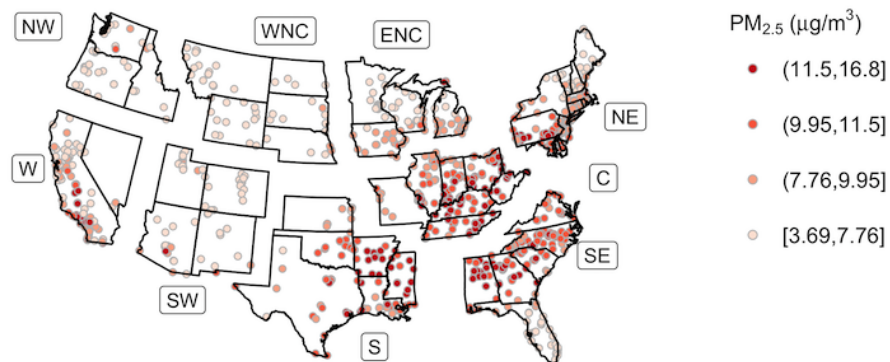
We apply our method to estimating the effect of wildfires on ambient $\text{PM}_{2.5}$ during 2008-2012 wildfire seasons in the contiguous U.S. We use these estimates to conduct a health burden analysis. Our Bayesian model provides full uncertainty quantification about the causal effects and resulting health burden assessment. While we apply the method to the example of wildfire-contributed $\text{PM}_{2.5}$, the approach is relevant to many applications.

2 Description of the $\text{PM}_{2.5}$ data

The analysis of fire-contributed $\text{PM}_{2.5}$ is conducted over the 2008 to 2012 wildfire seasons (May 1 - October 31) in the contiguous U.S. There are two sources of $\text{PM}_{2.5}$ data: monitor data from the Environmental Protection Agency's (EPA) Air Quality System (AQS) and simulated $\text{PM}_{2.5}$ from the CMAQ model. Both data sources cover the contiguous U.S., but because of the large size we partition the data into regions with similar climates and conduct the analysis separately by region (US EPA, 2018). In the Supplemental Materials (Section 2), we conduct a sensitivity analysis to demonstrate that model results are robust to blocking by region. The nine regions are displayed in Figure 1: West (W), Northwest

(NW), West North Central (WNC), East North Central (ENC), Northeast (NE), Central (C), Southeast (SE), South (S) and Southwest (SW).

Figure 1: **Summary of the monitor data.** The locations and daily $PM_{2.5}$ concentrations ($\mu\text{g}/\text{m}^3$) observed at EPA monitoring stations averaged over the 2008 to 2012 wildfire seasons. The breakpoints correspond to the 25th, 50th and 75th percentiles of $PM_{2.5}$.



2.1 AQS monitor data

We use $PM_{2.5}$ data from Federal Reference Method monitoring sites in the EPA AQS monitoring network. There are more monitors in urban areas than rural, since monitors in the AQS network are distributed according to population density (US Environmental Protection Agency, 2015). At each site, daily average concentrations of $PM_{2.5}$ are measured every one, three or six days. Figure 1 shows the monitor locations and the $PM_{2.5}$ observed at each monitor in the network averaged over the study time period. The observed average concentrations range from 3.69 to 16.8 $\mu\text{g}/\text{m}^3$. The highest concentrations of $PM_{2.5}$ are in California and the Southeast, and the lowest are in the West North Central and Southwest regions.

2.2 CMAQ model output

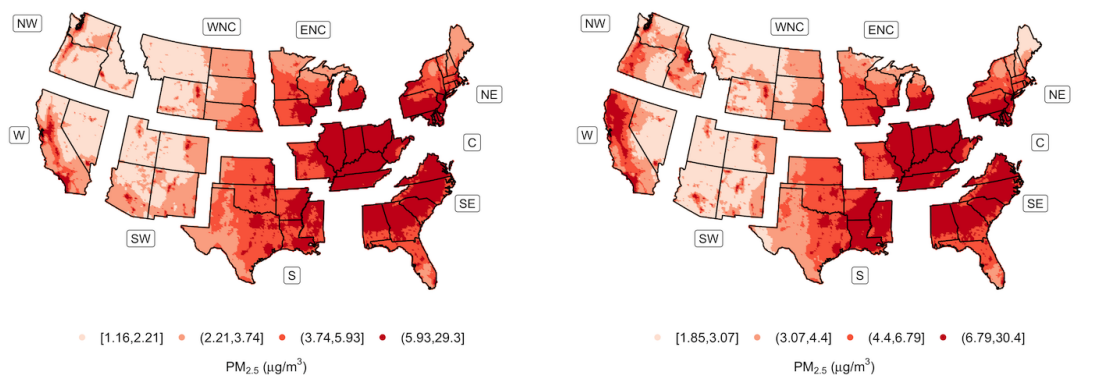
CMAQ is a deterministic model of air quality which represents the most important processes related to atmospheric chemistry using cutting-edge scientific knowledge. The model utilizes emissions from a wide range of sources and transport by winds to predict concentrations of ambient composition and deposition due to precipitation. CMAQ characterizes production and loss of hundreds of particle and gas phase pollutants (U.S. EPA, 2019). In the case of wildfire emissions, hourly information on fire location and size are determined using satellite information as well as on the ground reports. Wildland fire emissions are estimated based on the type, load, and conditions of vegetation at the detected burning site and uses vegetation-specific emission factors (U.S. Forest Service, 2019). The largest known sources of uncertainty arise due to misspecification in characterizing variability in weather patterns and anthropogenic emissions. In the case of wildfires, additional uncertainty arises from misclassification of plume rise, fire weather conditions and other factors.

The CMAQ-simulated $PM_{2.5}$ data is the average $PM_{2.5}$ concentrations for each day in the 2008 to 2012 wildfire seasons on a 12×12 km grid over the contiguous U.S.; see Rappold et al. (2017) for details. The model is run with and without the forcing for wildland fire emissions. The run without fire emissions is a CMAQ estimate of $PM_{2.5}$ in the counterfactual scenario where no wildland fires are possible. The difference in $PM_{2.5}$ concentrations between the two runs is a CMAQ estimate of fire-contributed $PM_{2.5}$. CMAQ captures emissions, topology, weather conditions, fate and transport of air pollution among other factors. However, there are many possible remaining determinants or knowledge gaps that lead to either error and bias, which motivates our statistical approach.

Figure 2 displays the $PM_{2.5}$ modeled by CMAQ averaged over the 2008 to 2012 wildfire seasons. The western half of the U.S. has predominantly low concentrations of $PM_{2.5}$ (1.16 - $2.21 \mu\text{g}/\text{m}^3$) when fire emissions are excluded, but higher concentrations when fire emissions are included (up to 6.78 - $30.4 \mu\text{g}/\text{m}^3$). This trend is particularly notable in the West and Northwest regions, where wildfire frequency is high and fire-contributed $PM_{2.5}$ comprises 23.5-91.8% of the total $PM_{2.5}$ in parts of these regions (i.e. central and northern

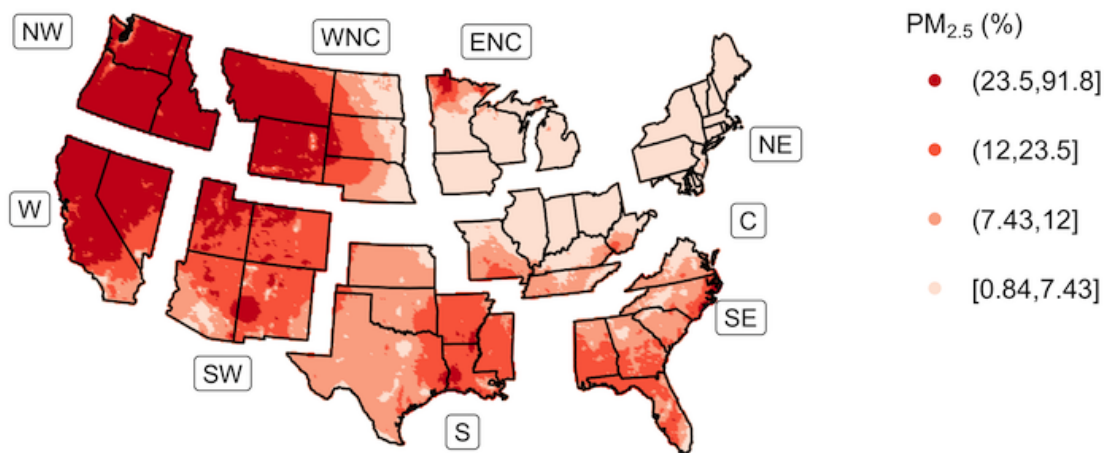
California, eastern Oregon and Washington, and central Idaho). In the South and Southeastern regions, contribution of both wildland and prescribed fires is evident. Figure 3 provides a time series of observed $PM_{2.5}$ concentrations and CMAQ estimates at a site in Northern California. On days where wildfire activity is present, CMAQ tends to produce higher estimates of total $PM_{2.5}$.

Figure 2: **Summary of the CMAQ-estimated PM_{2.5} concentrations.** The daily CMAQ PM_{2.5} concentrations ($\mu\text{g}/\text{m}^3$) averaged over the 2008 to 2012 fire seasons on a 12×12 km grid across the contiguous U.S. by region. Panel (a) displays average PM_{2.5} from the CMAQ run without fire emissions; Panel (b) displays average PM_{2.5} from the CMAQ run with fire emissions; and panel (c) shows the difference between these runs reported as the percentage of the total.



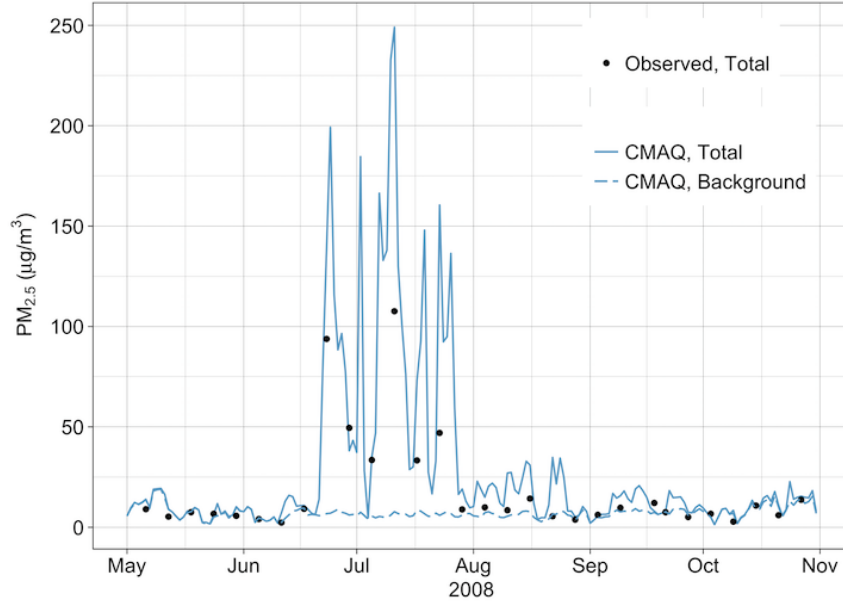
(a) PM_{2.5} without fires ($\mu\text{g}/\text{m}^3$)

(b) Total PM_{2.5} ($\mu\text{g}/\text{m}^3$)



(c) Fire-Contributed PM_{2.5} as % of Total PM_{2.5}

Figure 3: **Times series plot at one site.** Total $\text{PM}_{2.5}$ from CMAQ run with and without the forcing for fire emissions, and total $\text{PM}_{2.5}$ measured at an AQS monitoring site in Northern California ($-121.8^\circ, 39.8^\circ$) during the 2008 wildfire season.



3 Methods

3.1 Notation

We first establish some notation for the data. Let the observed monitor data be $Y_t(\mathbf{s})$ for day t and location $\mathbf{s} \in \mathcal{R}^2$ in spatial domain \mathcal{D} . We denote CMAQ output from the no-fire run as $\hat{\theta}_t(\mathbf{s})$ and the difference between the fire and no-fire runs as $\hat{\delta}_t(\mathbf{s})$. We denote other environmental factors that are related to both fire activity and $\text{PM}_{2.5}$ (confounders such as non-fire natural emissions, anthropogenic sources, wind, land type, etc.) as $X_t(\mathbf{s})$ and binary fire presence as $A_t(\mathbf{s})$, so that $A_t(\mathbf{s}) = 1$ if there is a fire burning at \mathbf{s} on day t and $A_t(\mathbf{s}) = 0$ otherwise. The smoke plumes associated with the fires determine which locations' air quality are affected by the fires, and so we define $C_t(\mathbf{s}) = 1$ if site \mathbf{s} is in

a plume on day t and $C_t(\mathbf{s}) = 0$ otherwise to capture spillover effects. The collection of data across space is denoted in bold, e.g. $\mathbf{A}_t = \{A_t(\mathbf{s}) : \mathbf{s} \in \mathcal{D}\}$ for the fire indicators.

3.2 Fire regimes and potential outcomes framework

To estimate fire-attributable $\text{PM}_{2.5}$, i.e., the amount of $\text{PM}_{2.5}$ that would not have occurred were it not for wildland fires, we use a potential outcomes framework (Rubin, 1978). To this end, we define regimes $R = 1$ and $R = 0$ over spatial domain \mathcal{D} : the fire regime ($R = 1$) under which wildfires occur in \mathcal{D} , and the no-fire regime ($R = 0$) under which fires do not occur anywhere in \mathcal{D} . We also define the potential $\text{PM}_{2.5}$ under regimes $R = 0$ and $R = 1$ as $Y_t(\mathbf{s}, 0)$ and $Y_t(\mathbf{s}, 1)$, respectively, and model each as

$$\begin{aligned} Y_t(\mathbf{s}, 0) &= \theta_t(\mathbf{s}), \\ Y_t(\mathbf{s}, 1) &= \theta_t(\mathbf{s}) + \delta_t(\mathbf{s}), \end{aligned} \tag{1}$$

where $\theta_t(\mathbf{s})$ and $\delta_t(\mathbf{s})$ are stochastic processes representing non-fire and fire-attributed $\text{PM}_{2.5}$, respectively.

Under regime $R = 1$ the potential outcomes are generated by sampling \mathbf{X}_t , $\mathbf{A}_t|\mathbf{X}_t$, $\mathbf{C}_t|\mathbf{A}_t, \mathbf{X}_t$, and finally $\mathbf{Y}_t(1)|\mathbf{X}_t, \mathbf{A}_t, \mathbf{C}_t$ in sequence. Similarly, under regime $R = 0$, the potential outcome are generated by sampling \mathbf{X}_t and then $\mathbf{Y}_t(0)|\mathbf{X}_t$ setting $\mathbf{A}_t = \mathbf{C}_t = 0$. Therefore, the amount of $\text{PM}_{2.5}$ caused by wildland fires is quantified by the average (over \mathbf{X}_t , \mathbf{A}_t and \mathbf{C}_t) difference in the potential outcomes (Rubin, 1978; Holland, 1986; Hernán et al., 2008):

$$\Delta(\mathbf{s}) = \text{E}[Y_t(\mathbf{s}, 1) - Y_t(\mathbf{s}, 0)] = \text{E}[\delta_t(\mathbf{s})].$$

In our analysis, we average over time throughout the entire fire season and years of the study, although this framework could be applied to estimate the causal effect annually, seasonally or even daily.

3.3 Assumptions

The fundamental problem in causal inference is that not all potential outcomes are observed for each \mathbf{s} and t (Holland, 1986). Therefore, the potential outcome models and the causal effect, $\Delta(\mathbf{s})$, are not identifiable without assumptions, which we discuss below.

We assume there exist bias-correction functions, B_0 and B_1 , and we observe binary indicator $C_t(\mathbf{s}) \in \{0, 1\}$ where \mathbf{s} is affected by wildfire smoke if and only if $C_t(\mathbf{s}) = 1$ so that the following hold:

Assumption 1 (Potential Outcomes Model). *The counterfactual processes can be decomposed as,*

$$\theta_t(\mathbf{s}) = B_0(\hat{\theta}_t(\mathbf{s}), \mathbf{s}) + e_{0t}(\mathbf{s}) \quad \text{and} \quad \delta_t(\mathbf{s}) = B_1(\hat{\delta}_t(\mathbf{s}), \mathbf{s}) + e_{1t}(\mathbf{s}),$$

where $[e_{0t}(\mathbf{s}), e_{1t}(\mathbf{s})]$ is a bivariate spatial process independent of \mathbf{X}_t , \mathbf{A}_t and \mathbf{C}_t given $\hat{\theta}_t$ and $\hat{\delta}_t$.

The bias correction functions B_0 and B_1 can be flexible nonlinear functions (e.g., splines) and vary by spatial location and the discrepancy terms e_{0t} and e_{1t} account for model misspecification and are modeled as spatial processes (Kennedy and O’Hagan, 2001). To allow for learning where the model is under-performing relative to the truth, we model CMAQ bias function B_j to be a flexible spatially varying surface. As such, this bias function enables us to gain insights into possible spatially-varying confounding by examining the residual variation.

Equation (1) and Assumption 1 specify the full joint model between counterfactual outcomes $Y_t(\mathbf{s}, 0)$ and $Y_t(\mathbf{s}, 1)$ given $[\hat{\theta}_t(\mathbf{s}), \hat{\delta}_t(\mathbf{s})]$. Under Assumption 1, $[Y_t(\mathbf{s}, 0), Y_t(\mathbf{s}, 1)]$ are independent of \mathbf{X}_t given $[\hat{\theta}_t(\mathbf{s}), \hat{\delta}_t(\mathbf{s})]$. Therefore, $[\hat{\theta}_t(\mathbf{s}), \hat{\delta}_t(\mathbf{s})]$ can be called the prognostic score of Hansen (2008), which is the prognostic analogue of the propensity score. Also, Assumption 1 implies that all confounders with the regime realizations and potential outcomes are captured through CMAQ output, since Assumption 1 implies $[\theta_t(\mathbf{s}), \delta_t(\mathbf{s})]$, and thus $[Y_t(\mathbf{s}, 0), Y_t(\mathbf{s}, 1)]$, are independent of \mathbf{C}_t given $[\hat{\theta}_t(\mathbf{s}), \hat{\delta}_t(\mathbf{s})]$. This is similar to the unconfounded network influence assumption of Kao (2017) under the social network

framework. Although Assumption 1 is key for identification and dramatically simplifies the analysis compared to modeling the effect of \mathbf{X}_t , it cannot be verified from the observed data. Because CMAQ uses most important meteorological and environmental factors for fire activity, smoke transportation, and $\text{PM}_{2.5}$ as well as state-of-the-art computer simulations (see Section 2.2), this assumption is plausible.

Assumption 2 (Consistency). *Ignoring measurement errors, the observation at \mathbf{s} equals the potential outcome at \mathbf{s} under regime given by $C_t(\mathbf{s})$,*

$$Y_t(\mathbf{s}) = \begin{cases} Y_t(\mathbf{s}, 0), & \text{if } C_t(\mathbf{s}) = 0, \\ Y_t(\mathbf{s}, 1), & \text{if } C_t(\mathbf{s}) = 1. \end{cases}$$

Assumption 2 links the potential outcomes with the observed outcomes. In particular, it allows for partial realizations of $Y_t(\mathbf{s}, 0)$ removing the need to actualize a situation under the counterfactual no-fire regime. For example, this assumption implies that a set of monitors far removed from fires and plumes on day t can be assumed to follow the potential outcomes distribution under the no fires regime and thus be used to identify parameters in this distribution such as those that determine B_0 and the spatial covariance of $e_{0t}(\mathbf{s})$. As long as an appropriate variable $C_t(\mathbf{s})$ can be identified from the observed data, this assumption is plausible. In our analysis we use CMAQ output to determine $C_t(\mathbf{s})$. Namely, we let $C = 1(\hat{\delta} > \tau)$, where τ is a fixed threshold chosen through cross-validation and sensitivity analysis.

Theorem 1 gives the main identification result with the proof deferred to the Appendix.

Theorem 1. *Under Assumptions 1 and 2 and further assuming that \mathbf{C}_t is not degenerate, the parameters in the potential outcome models are identifiable via the distribution of the observed data, i.e. the distribution of \mathbf{Y}_t given $(\hat{\boldsymbol{\theta}}_t, \hat{\boldsymbol{\delta}}_t, \mathbf{C}_t)$.*

While we never observe complete \mathbf{Y}_t (i.e., for all \mathbf{s}) under the no fires regime, Assumptions 1 and 2 along with the non-degeneracy of \mathbf{C}_t are sufficient for identification. By Theorem 1, causal parameter estimation only requires inspecting the implied model for $Y_t(\mathbf{s})$ and confirming parameter identification. In Section 3.4 we specify parametric models for the

bias correction functions B_0 and B_1 and the spatial process $\mathbf{e}_t(\mathbf{s}) = [e_{0t}(\mathbf{s}), e_{1t}(\mathbf{s})]^T$. We then argue in Section 3.5 that all parameters, including the correlation between counterfactuals, are identifiable in our spatial setting. This setup serves as a basis for using a Bayesian approach to estimating the causal effect, $\Delta(\mathbf{s})$.

Defining the intervention as the fire regime instead of individual fires ($A_t(\mathbf{s})$) is key for two reasons. First, this is parallel to how the numerical model simulates fire and no-fire $\text{PM}_{2.5}$. Second, the amount of fire-contributed $\text{PM}_{2.5}$ at any site in the spatial domain depends on the fire status at other sites, because the smoke from fires at neighboring sites is transported. This is called interference or spill-over and it is problematic because we could not reasonably claim that changes in $\text{PM}_{2.5}$ at site \mathbf{s} were only due to fire presence or absence at site \mathbf{s} , i.e., $Y_t(\mathbf{s}, A_t(\mathbf{s}))$ is not well-defined. There would be a different potential outcome for every possible \mathbf{A}_t , resulting in 2^n potential outcomes per site for a spatial domain containing n sites.

3.4 Bayesian hierarchical model

Assumption 1 and the addition of measurement error give the following model for the observed $\text{PM}_{2.5}$:

$$Y_t(\mathbf{s}) = \theta_t(\mathbf{s}) + C_t(\mathbf{s})\delta_t(\mathbf{s}) + \epsilon_t(\mathbf{s}), \quad (2)$$

where $\epsilon_t(\mathbf{s}) \stackrel{iid}{\sim} \mathcal{N}(0, \sigma^2)$ are measurement errors. To separate background $\text{PM}_{2.5}$ from fire-contributed $\text{PM}_{2.5}$, we assign priors to $\theta_t(\mathbf{s})$ and $\delta_t(\mathbf{s})$ based on bias-adjusted CMAQ runs, as per Assumption 1. We model the means of both processes as

$$B_j(z, \mathbf{s}) = \alpha_j(\mathbf{s}) + \beta_j(\mathbf{s})z$$

for $j = 0, 1$, where $\alpha_j(\mathbf{s})$ is the additive bias and $\beta_j(\mathbf{s})$ is the multiplicative bias. The bias terms have Gaussian process priors with means $\mathbb{E}[\alpha_j(\mathbf{s})] = \mu_{\alpha_j}$ and $\mathbb{E}[\beta_j(\mathbf{s})] = \mu_{\beta_j}$ and covariances $\text{Cov}[\alpha_j(\mathbf{s}), \alpha_j(\mathbf{s}')] = \sigma_{\alpha_j}^2 \exp(-\|\mathbf{s} - \mathbf{s}'\|/\phi_2)$ and $\text{Cov}[\beta_j(\mathbf{s}), \beta_j(\mathbf{s}')] =$

$\sigma_{\beta_j}^2 \exp(-\|\mathbf{s} - \mathbf{s}'\|/\phi_2)$. The prior distributions for all hyper-parameters are detailed in Appendix B.

The background and fire-contributed $\text{PM}_{2.5}$ then have the following form:

$$\begin{aligned}\theta_t(s) &= \alpha_0(\mathbf{s}) + \beta_0(\mathbf{s})\hat{\theta}_t(\mathbf{s}) + e_{0t}(\mathbf{s}), \\ \delta_t(s) &= \alpha_1(\mathbf{s}) + \beta_1(\mathbf{s})\hat{\delta}_t(\mathbf{s}) + e_{1t}(\mathbf{s}),\end{aligned}\tag{3}$$

where $\mathbf{e}_t(\mathbf{s}) = [e_{0t}(\mathbf{s}), e_{1t}(\mathbf{s})]^T$ is a bivariate spatial process with mean $\mathbb{E}[e_{jt}(\mathbf{s})] = 0$ and separable exponential covariance $\text{Cov}[\mathbf{e}_t(\mathbf{s}), \mathbf{e}_t(\mathbf{s}')] = \Sigma \exp(-\|\mathbf{s} - \mathbf{s}'\|/\phi_1)$. The 2×2 cross-covariance matrix Σ has diagonal elements σ_1^2 and σ_2^2 , and off-diagonal element $\sigma_{12} = \sigma_1\sigma_2\gamma$, so γ gives the correlation between counterfactual outcomes.

3.5 Estimability

In this section, we argue that all parameters in the joint model specified above are estimable.

Consider the parameters in the mean,

$$E[Y_t(\mathbf{s})] = \mu_t(\mathbf{s}) = \alpha_0(\mathbf{s}) + \beta_0(\mathbf{s})\hat{\theta}_t(\mathbf{s}) + \alpha_1(\mathbf{s})C_t(\mathbf{s}) + \beta_1(\mathbf{s})[C_t(\mathbf{s})\hat{\delta}_t(\mathbf{s})].\tag{4}$$

Assuming the four covariates $(1, \hat{\theta}_t(\mathbf{s}), C_t(\mathbf{s}), C_t(\mathbf{s})\hat{\delta}_t(\mathbf{s}))$ are not linearly dependent at \mathbf{s} , then the four parameters $\alpha_0(\mathbf{s})$, $\alpha_1(\mathbf{s})$, $\beta_0(\mathbf{s})$ and $\beta_1(\mathbf{s})$ are estimable. For example, ordinary least squares would provide an unbiased and consistent estimator (as the number of days increases). This result clearly relies on Assumption 1 or it would not be possible to identify both $\alpha_0(\mathbf{s})$ and $\alpha_1(\mathbf{s})$.

Under the model $Y_t(\mathbf{s}) = \mu_t(\mathbf{s}) + e_{0t}(\mathbf{s}) + C_t(\mathbf{s})e_{1t}(\mathbf{s}) + \epsilon_t(\mathbf{s})$, the covariance is

$$\text{Cov}[Y_t(\mathbf{s}), Y_t(\mathbf{s}') | \hat{\theta}_t(\mathbf{s}), \hat{\delta}_t(\mathbf{s})] = \begin{cases} \sigma_1^2 \exp(-h/\phi_1) & \text{if } C_t(\mathbf{s}) = C_t(\mathbf{s}') = 0 \\ \sigma_1^2(1 + \frac{\sigma_2}{\sigma_1}\gamma) \exp(-h/\phi_1) & \text{if } C_t(\mathbf{s}) \neq C_t(\mathbf{s}') \\ (\sigma_1^2 + 2\sigma_1\sigma_2\gamma + \sigma_2^2) \exp(-h/\phi_1) & \text{if } C_t(\mathbf{s}) = C_t(\mathbf{s}') = 1, \end{cases}\tag{5}$$

where $h = \|\mathbf{s} - \mathbf{s}'\|$. By examining the spatial correlation between pairs of points separately according to their values of $C_t(\mathbf{s})$, the parameters σ_1^2 , σ_2^2 , γ and ϕ_1 are estimable. For example, simple variogram-based methods could be used to estimate these parameters. More importantly, under the full Bayesian model, $\text{Cov}[Y_t(\mathbf{s}, 0), Y_t(\mathbf{s}, 1) | Y_t(\mathbf{s})] = \sigma_1^2(1 + \frac{\sigma_2}{\sigma_1}\gamma)$ is estimable, although $Y_t(\mathbf{s}, 0)$ and $Y_t(\mathbf{s}, 1)$ are never jointly observed at one location. In our analysis we use Bayesian modeling to jointly estimate the mean and covariance parameters.

3.6 Posterior inference

The causal effect at \mathbf{s} is approximated as,

$$\Delta(\mathbf{s}) \approx \frac{1}{T} \sum_{t=1}^T C_t(\mathbf{s}) \delta_t(\mathbf{s}).$$

Our fully Bayesian analysis produces the entire posterior distribution of the causal effect, including the posterior mean $\bar{\Delta}(\mathbf{s}) = \frac{1}{T} \sum_{t=1}^T C_t(\mathbf{s}) \bar{\delta}_t(\mathbf{s})$, where $\bar{\delta}_t(\mathbf{s})$ is the posterior mean of $\delta_t(\mathbf{s})$. The estimate, $\bar{\delta}_t(\mathbf{s})$, includes both bias-corrected CMAQ, $B_0(\hat{\theta}_t(\mathbf{s}), \mathbf{s})$ and $B_1(\hat{\delta}_t(\mathbf{s}), \mathbf{s})$, and observed data, $Y_t(\mathbf{s})$, allowing us to account for any daily variation in fire-attributable $\text{PM}_{2.5}$ not captured by CMAQ. Finally, $\bar{\delta}_t(\mathbf{s})$ is based on estimable parameters defined in the previous section, making $\bar{\Delta}(\mathbf{s})$ an estimable quantity as well.

We multiply $\bar{\delta}_t(\mathbf{s})$ by $C_t(\mathbf{s})$ because given Assumption 2, this relates the observations to the potential outcomes, thereby imparting the causal interpretation on $\bar{\Delta}(\mathbf{s})$. Multiplying by $C_t(\mathbf{s})$ also allows the model to only identify $\delta_t(\mathbf{s})$ as a causal quantity if $C_t(\mathbf{s}) = 1$, which is important as we are not interested in the $\text{PM}_{2.5}$ if there were fires affecting \mathbf{s} every day, but the causal estimate if the fires we observed were removed.

Assuming conditional independence of $C_t(\mathbf{s})$ and $\delta_t(\mathbf{s})$ given $Y_t(\mathbf{s}), \hat{\theta}_t(\mathbf{s}), \hat{\delta}_t(\mathbf{s})$ over time, $\bar{\Delta}(\mathbf{s})$ satisfies

$$\begin{aligned} E[\bar{\Delta}(\mathbf{s})] &= E[C_t(\mathbf{s}) \bar{\delta}_t(\mathbf{s})] \\ &= E[C_t(\mathbf{s}) E[\delta_t(\mathbf{s}) | Y_t(\mathbf{s}), \hat{\theta}_t(\mathbf{s}), \hat{\delta}_t(\mathbf{s})]] \\ &= E[C_t(\mathbf{s}) \delta_t(\mathbf{s})]. \end{aligned}$$

Hence it is reasonable to use $\bar{\Delta}(\mathbf{s})$ to approximate the causal effect.

3.7 Computation

To approximate the posterior of the causal effect $\Delta(\mathbf{s})$, we implement the spatial Bayesian analysis using a Markov chain Monte Carlo sampling. The missing values of observed $\text{PM}_{2.5}$ are imputed and every model parameter is iteratively updated by the algorithm, conditional on all other parameters. The spatial range parameters, ϕ_1 and ϕ_2 are estimated empirically using variograms. All other model parameters have conditionally-conjugate priors and are accordingly updated with Gibbs steps where each step samples from their respective full conditional distributions (see Appendix B.1 for derivations of the full conditional distributions). We use Gaussian Kriging to estimate smooth spatial surfaces across each study region for both the posterior means and standard deviations of each model parameter. We Kriged each estimate to the centroids of the 12×12 km CMAQ grid. Our MCMC has a burn-in period of length 5,000, after which we collect samples every 100 iterations until a total of 30,000 iterations have been completed. To verify that the MCMC algorithm converged, we computed the effective sample size of the causal effect estimate, $\Delta(\mathbf{s})$, for each \mathbf{s} . We also monitored convergence using visual inspection of trace plots for several representative parameters. Summary statistics and figures of the effective sample sizes and trace plots are included in the Supplemental Materials, Section 1.

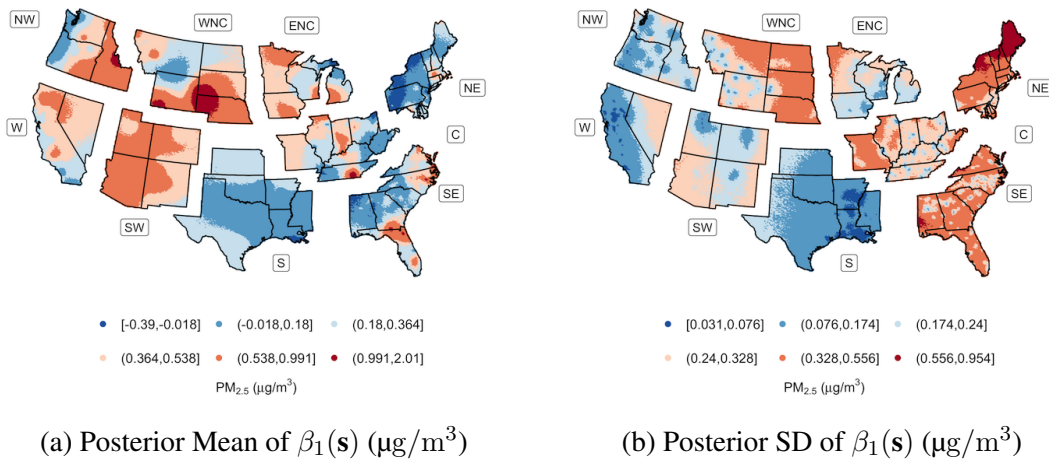
4 Fire-contributed $\text{PM}_{2.5}$ estimates

We let $C_t(\mathbf{s}) = I[\hat{\delta}_t(\mathbf{s}) > \tau]$, where $\hat{\delta}_t(\mathbf{s})$ is the CMAQ estimate of fire-attributed $\text{PM}_{2.5}$ and τ is a fixed threshold. To select the threshold, we ran several models for a range of values of τ and used five-fold cross-validation to evaluate each model's ability to predict total $\text{PM}_{2.5}$. We found little variation between the prediction metrics between each model. For example, mean-squared error (MSE) ranged from $12.58\mu\text{g}/\text{m}^3$ ($\tau = 1\mu\text{g}/\text{m}^3$) to $12.71\mu\text{g}/\text{m}^3$ ($\tau = 5\mu\text{g}/\text{m}^3$) (Supplemental Materials, Section 4, Table 1). We also examined variation in the causal effect when estimated with different values of τ and found

the differences to be negligible except if τ is selected to be extreme (e.g. 0 or 10 $\mu\text{g}/\text{m}^3$) (Supplemental Materials, Section 4, Figure 5). Based on these findings, we concluded that the model is robust to moderate choices for the threshold and we let $\tau = 1\mu\text{g}/\text{m}^3$ for the remaining analysis.

Figure 4 shows the posterior mean and standard deviation for the multiplicative bias parameter for the fire-contribution process, $\beta_1(\mathbf{s})$. Similar maps for the other bias parameters are included in Appendix B.2. The highest 2nd percent of $\beta_1(\mathbf{s})$ values reached (0.991, 2.01 $\mu\text{g}/\text{m}^3$), meaning that the strongest estimated association between CMAQ estimates and the monitor data occurs in the Northwest and West North Central (WNC) regions, along with parts of the East North Central region, the Southwest and parts of the Southeast region (Figure 4). The lowest values (-0.39, -0.018 $\mu\text{g}/\text{m}^3$) in the northern part of the East North Central region, the South and parts of the Northeast region. These have fewer wildfires (Figure 2) and thus it is more difficult for CMAQ to estimate the relationship between model-estimated contribution and observed $\text{PM}_{2.5}$. This is neither surprising nor problematic because these regions rarely experience fire smoke.

Figure 4: **Maps of the bias terms.** Posterior means and standard deviations (SD) of the multiplicative bias for CMAQ’s fire-contributed $\text{PM}_{2.5}$, $\beta_1(\mathbf{s})$. The breakpoints correspond to the 2nd, 25th, 50th, 75th and 98th percentiles.



The posterior mean of the correlation between the counterfactual processes is summarized in Figure 5. Observing a positive correlation in a given region is indicative of fire smoke occurring in areas where non-fire $\text{PM}_{2.5}$ emissions are present. A negative correlation indicates the converse. The highest estimated correlation is in the West region (0.44 ± 0.05), followed by the WNC region (0.31 ± 0.15) and then the South, Central and Southeast regions ($0.26 \pm 0.08, 0.26 \pm 0.06, 0.25 \pm 0.02$). The Northeast region exhibits low correlation (0.16 ± 0.04). The correlation estimate for the Southwest region (-0.21 ± 0.06) is negative, and the only areas for which the correlation was plausibly zero were the ENC and the Northwest regions. To further illustrate the spatial correlation between observations, we also provide plots of Equation 5 evaluated at the posterior mean of the model parameters for each region and combination of $C_t(\mathbf{s})$ in the Supplemental Materials (Section 3, Figure 4).

Figure 5: **Correlation and 95% credible intervals.** The posterior means and 95% credible intervals of γ , the correlation between $\theta_t(\mathbf{s})$ and $\delta_t(\mathbf{s})$.

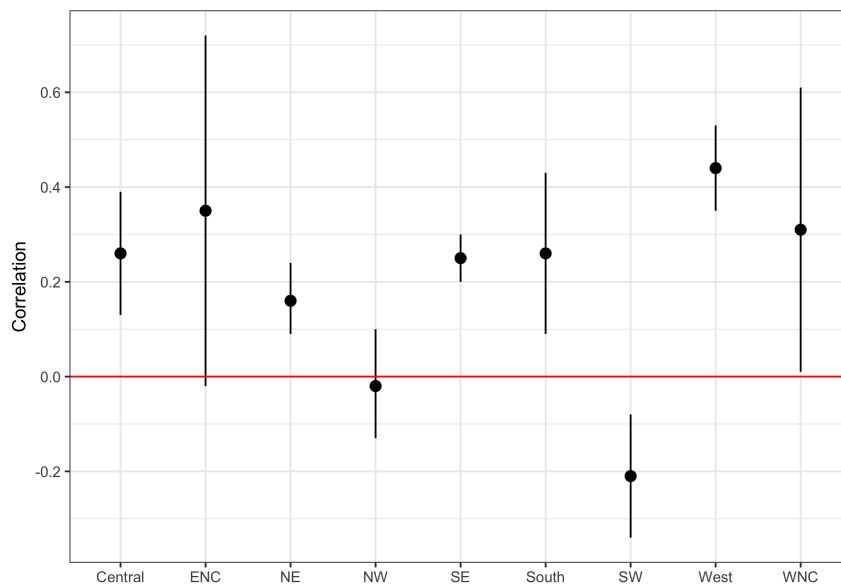


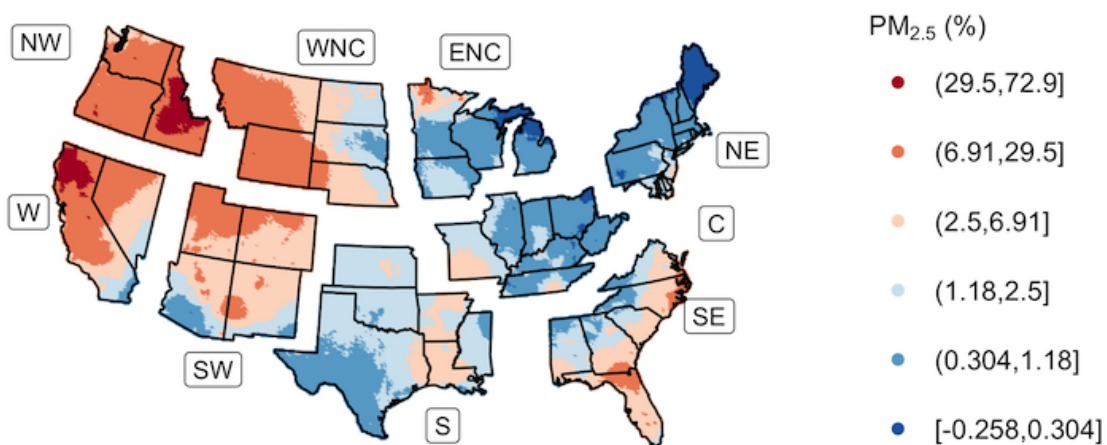
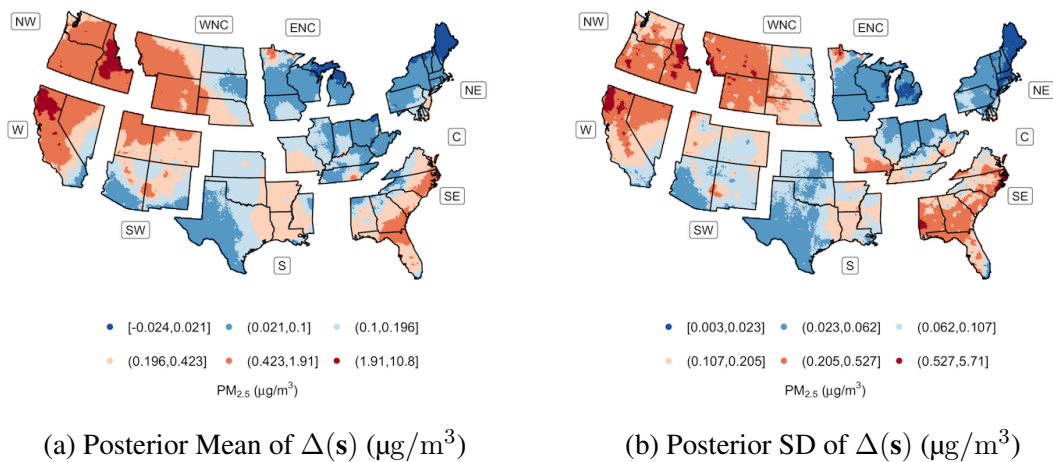
Figure 6 displays the causal effect estimates (Panel a), posterior standard deviation

(Panel b) and the causal effect as percent of total estimated $PM_{2.5}$ (Panel c). The largest estimates occur in the West, Northwest and WNC regions where wildfires are most prevalent. In these areas, between 29.5% and 72.9% of $PM_{2.5}$ is attributable to wildfire smoke (Figure 6c). Moderate effects are estimated in areas of the South and Southeast, where prescribed burning is prevalent. The causal estimates in the East North Central region are in both the top and bottom two percent of fire-contributed $PM_{2.5}$. This area is typically only effected by long-range smoke transport from the western U.S. or from Canadian wildland fires further north. Large areas of the Northeast region have estimates near zero (some locations have very small negative values, likely due to statistical uncertainty).

Figure 6 shows Bayesian model estimates of background and total $PM_{2.5}$, CMAQ-simulated background and total $PM_{2.5}$, as well as observed $PM_{2.5}$ during the 2008 wildfire season. Although the spatial pattern of the causal estimates resembles the CMAQ estimates, there are notable differences in the range of the estimates. Figure 7 illustrates these differences at the same site on Northern California shown in Figure 3. The estimates from the Bayesian causal model tend to fit closely to the observed values of $PM_{2.5}$ from the monitor rather than to the CMAQ-simulated total $PM_{2.5}$ and that the CMAQ model estimates are, on average, much higher.

We also compare the estimates from the Bayesian causal model to those from CMAQ for all monitoring sites (Figure 8) and the prediction sites (Figure 9). As in Figure 7, the Bayesian model generally produces lower estimates of fire-contributed $PM_{2.5}$ than CMAQ at all regions, both at monitoring sites (Figure 8) and prediction sites (Figure 9). The 95% credible intervals are longer at the prediction locations than at the monitoring sites, which is to be expected in an interpolation analysis. Additionally, only in regions where fires are prevalent (e.g., West, Northwest, WNC) do we see causal effect estimates significantly different from zero.

Figure 6: **Causal effect estimate.** The maps show the posterior mean and standard deviation of the causal effects, $\Delta(s)$. Values are averaged over the 2008 to 2012 wildfire seasons at each site.



(c) Fire-Contributed PM_{2.5} as % of Total PM_{2.5}

Figure 7: **Times series plot of estimates for one site.** Background ($\hat{\theta}_t(\mathbf{s})$) and total $\text{PM}_{2.5}$ ($\hat{\theta}_t(\mathbf{s}) + \hat{\delta}_t(\mathbf{s})$) from CMAQ, the posterior mean from the Bayesian model for background ($\theta_t(\mathbf{s})$) and total $\text{PM}_{2.5}$ ($\theta_t(\mathbf{s}) + C_t(\mathbf{s})\Delta_t(\mathbf{s})$), and the station measurements for an AQS site in Northern California ($-121.8^\circ, 39.8^\circ$) during the 2008 wildfire season.

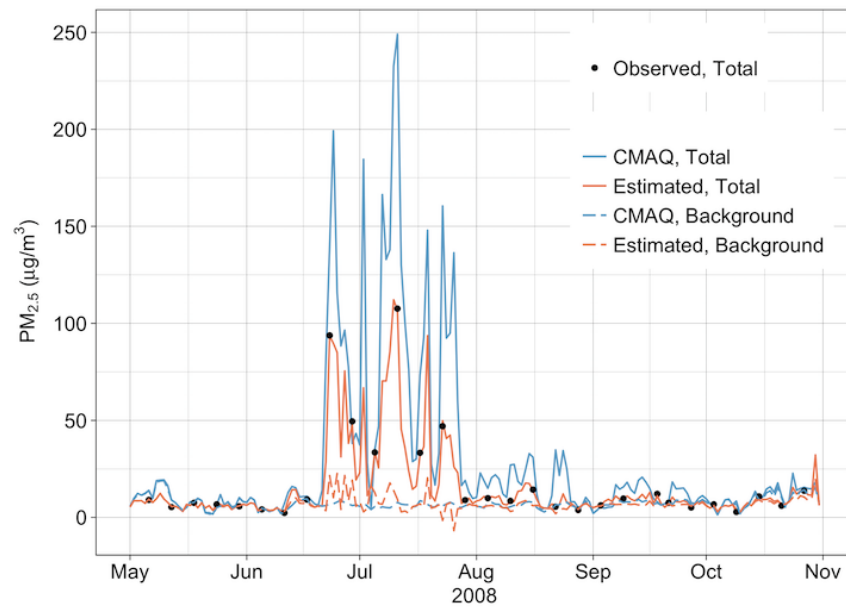
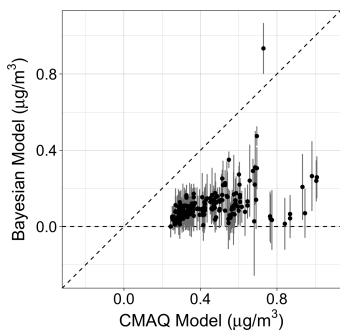
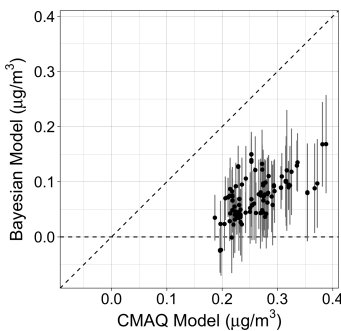


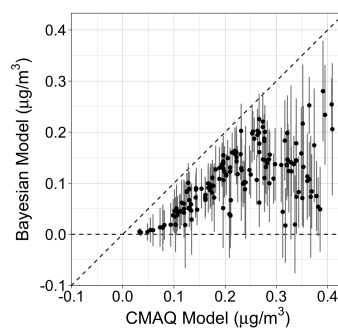
Figure 8: **Causal estimates at monitoring stations.** Fire-contributed $PM_{2.5}$ from the Bayesian model ($\Delta(s)$) versus the CMAQ model ($\hat{\delta}(s)$) at the AQS monitoring sites. Vertical error bars denote 95% credible intervals. The dashed lines represent $x = y$ and $y = 0$.



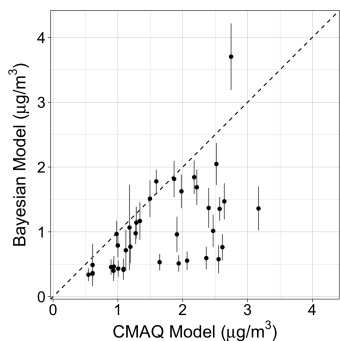
(a) Central



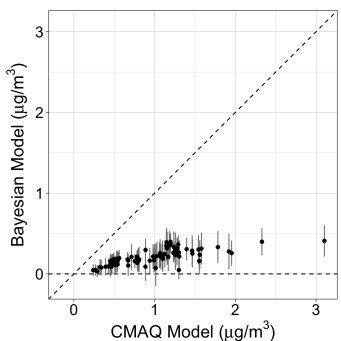
(b) East North Central



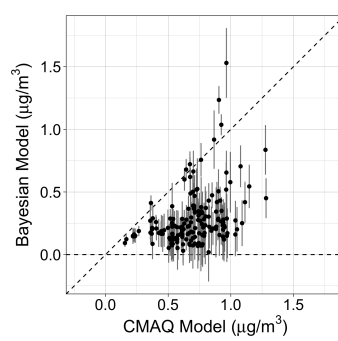
(c) Northeast



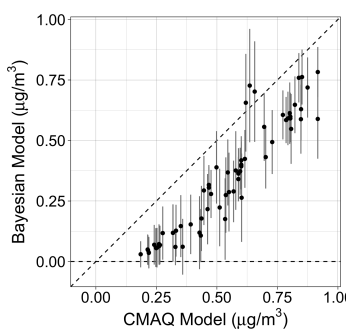
(d) Northwest



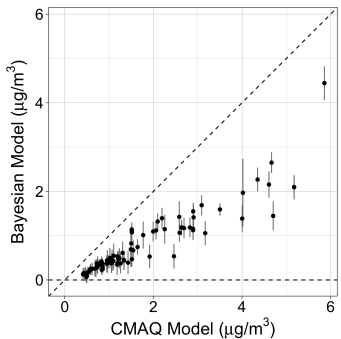
(e) South



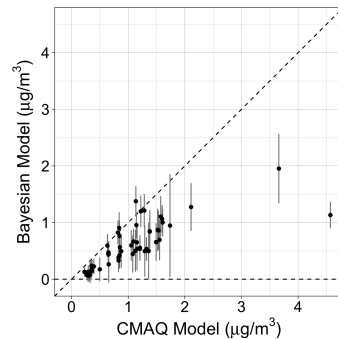
(f) Southeast



(g) Southwest

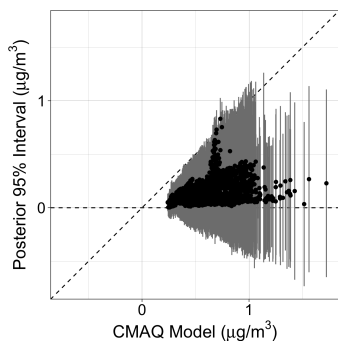


(h) West

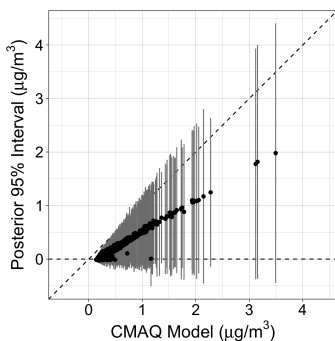


(i) West North Central

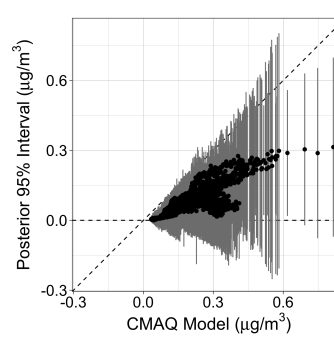
Figure 9: Causal estimates at prediction sites. Fire-contributed $PM_{2.5}$ from the Bayesian model versus the CMAQ model kriged to the 12×12 km CMAQ grid. Vertical error bars denote 95% credible intervals. The dashed lines represent $x = y$ and $y = 0$.



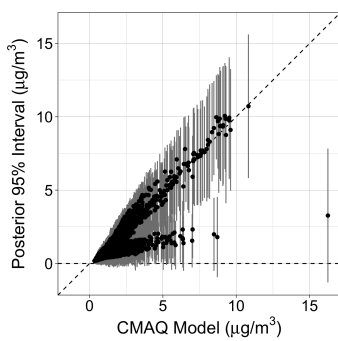
(a) Central



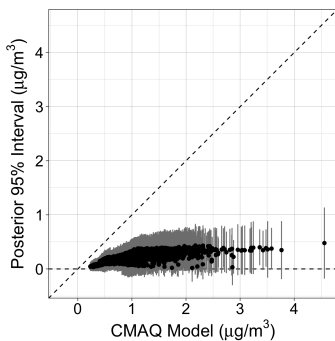
(b) East North Central



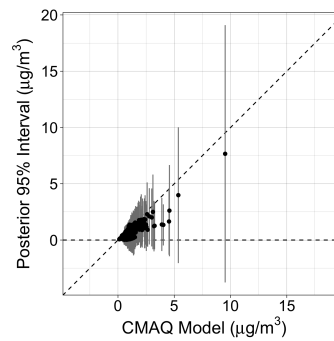
(c) Northeast



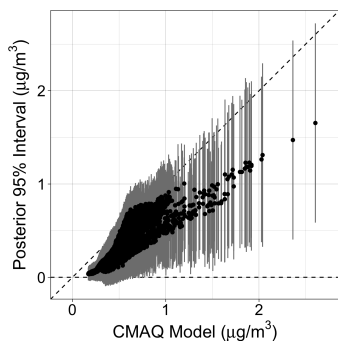
(d) Northwest



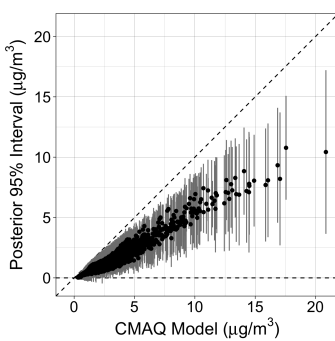
(e) South



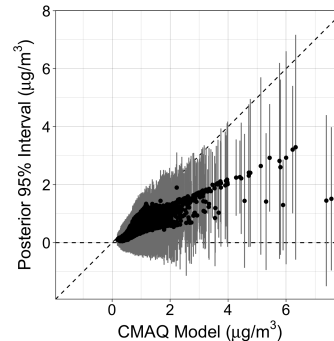
(f) Southeast



(g) Southwest



(h) West



(i) West North Central

5 Health burden analysis

We use a log-linear concentration-response function to describe the relationship between $\text{PM}_{2.5}$ and the number of hospitalizations due to respiratory illness. This analysis is conducted at the county level as well as by age group, a . We define Δ_c as the integrated causal effect $\Delta(\mathbf{s})$ for \mathbf{s} in county c . The health impact function relating fire-contributed $\text{PM}_{2.5}$ to changes in the incidence rate of hospitalizations due to respiratory illness is

$$R_{ac} = r_a^0 n_c (e^{r_a \Delta_c} - 1)$$

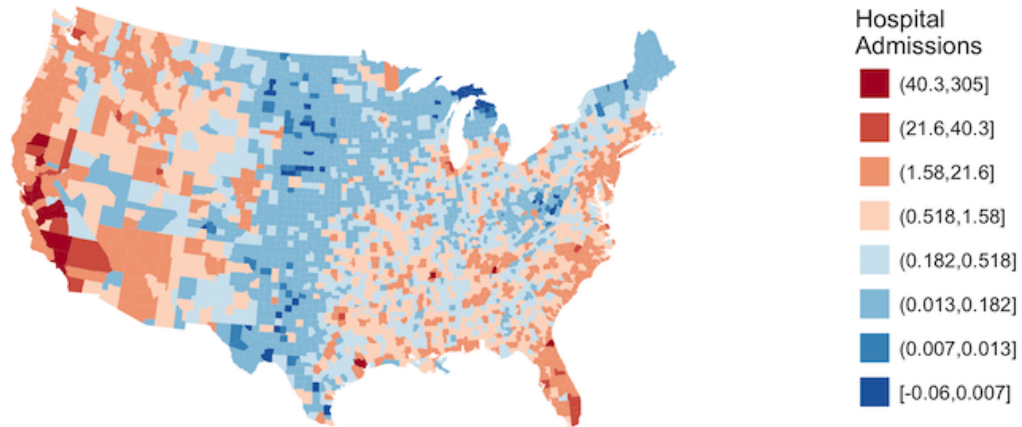
where n_c is the population of county c based on the July 2010 U.S. Census and r_a^0 is the incidence rate of hospitalizations for respiratory illness by county and age group (BenMAP, 2017). Using r_a , we calculate cumulative daily burden over all days in the study (May-October, 2008-2012) by county and age group (Figure 10) (Delfino et al., 2009). Cumulative R_{ac} over all counties in each region is summarized in Table 1 based on both the Bayesian and the CMAQ estimate of fire-contributed $\text{PM}_{2.5}$. We note that these estimates have a causal interpretation only if the estimates in Delfino et al. (2009) have a causal interpretation. While Delfino et al. (2009) account for many known confounders for fire-contributed $\text{PM}_{2.5}$ and respiratory illness and the U.S. EPA (2009) declares that the adverse effects of short-term $\text{PM}_{2.5}$ exposure on respiratory outcomes is likely to be causal (using the Hill criteria), this remains an important caveat.

The Bayesian estimate yields more conservative estimates of the impact of fire-contributed $\text{PM}_{2.5}$ on hospital admission rates for respiratory illness. The highest estimated burden is observed in the West region, notably in Southern California with upwards of 300 hospitalizations estimated cumulatively over the 2008 to 2012 fire seasons in some counties (Figure 10). In Table 1, the highest estimated burden for any region is in the West with 1513.9 hospitalizations over the 2008-2012 fire seasons using the Bayesian estimate of the causal effect. If the CMAQ estimate for the causal effect is used, the cumulative burden in the West is estimated to be 3500.4 hospitalizations per day. Most counties in the rest of the country exhibit lower burden with less than 5 hospitalizations per county over the 2008-2012 fire seasons (Figure 10).

Table 1: **Number of hospitalizations in each region.** Cumulative number of hospitalizations for respiratory illness due to wildland fires over the 2008-2012 fire seasons in each region calculated using the Bayesian and the CMAQ estimate of the causal effect, $\Delta_i(s)$, by region. 95% confidence intervals are provided.

Region	Δ	Age Group (years)				
		0-1	2-34	35-64	65-99	0-99
Central	Bayesian	150.5 (33.9, 270.6)	60.1 (-19.5, 146.6)	159.8 (33.5, 290.7)	283.7 (104.8, 460.1)	654.1 (152.7, 1168.0)
	CMAQ	612.8 (137.7, 1103.6)	242.3 (-77.9, 592.1)	663.5 (139.1, 1208.7)	1161.1 (428.4, 1884.9)	2679.8 (627.4, 4789.3)
ENC	Bayesian	26.7(6.0, 48.2)	10.4 (-3.4, 25.4)	28.5 (6.0, 52.0)	56.3 (20.8, 91.4)	121.9 (29.3, 217.1)
	CMAQ	95.4 (21.4, 172.3)	37.1 (-12.0, 91.1)	103.7 (21.7, 189.1)	207.7 (76.6, 337.5)	443.9 (107.7, 790.0)
South	Bayesian	134.9 (30.4, 242.1)	47.8 (-15.4, 116.2)	127.3 (26.7, 231.5)	248.9 (92.0, 403.4)	558.9 (133.8, 993.1)
	CMAQ	604.0 (135.1, 1093.7)	211.0 (-67.2, 518.7)	562.1 (117.5, 1027.1)	1102.0 (405.4, 1794.2)	2479.1 (590.8, 4433.7)
Southeast	Bayesian	279.3 (62.4, 506.0)	118.7 (-37.1, 290.9)	324.8 (67.9, 593.3)	565.6 (208.2, 920.5)	1288.3 (301.4, 2310.6)
	CMAQ	642.5 (144.1, 1160.6)	272.7 (-86.8, 667.4)	746.6 (156.4, 1361.3)	1284.4 (473.4, 2087.2)	2946.1 (687.1, 5276.5)
Southwest	Bayesian	113.6 (25.5, 205.1)	33.8 (-13.1, 85.4)	49.1 (10.3, 89.4)	85.6 (31.6, 139.1)	282.1 (54.2, 519.2)
	CMAQ	183.6 (41.2, 330.8)	57.3 (-21.7, 144.0)	89.3 (18.7, 162.7)	157.0 (58.0, 254.9)	487.3 (96.2, 892.4)
Northeast	Bayesian	116.5 (26.1, 210.1)	51.1 (-18.0, 127.0)	118.4 (24.8, 215.7)	231.6 (85.4, 376.2)	517.6 (118.4, 929.1)
	CMAQ	209.9 (47.3, 377.1)	93.2 (-32.2, 229.6)	231.0 (48.5, 420.2)	456.2 (168.5, 739.6)	990.3 (232.1, 1766.5)
Northwest	Bayesian	101.8 (22.6, 185.2)	40.5 (-11.6, 98.6)	116.0 (24.2, 212.5)	217.0 (79.7, 354.2)	475.3 (114.9, 850.6)
	CMAQ	184.1 (40.4, 340.9)	72.6 (-20.0, 179.5)	213.3 (44.1, 394.3)	401.5 (146.1, 661.3)	871.5 (210.6, 1575.9)
West	Bayesian	391.9 (86.3, 722.1)	142.5 (-51.0, 365.2)	312.8 (64.7, 578.4)	666.7 (242.7, 1097.7)	1513.9 (342.7, 2763.3)
	CMAQ	906.3 (195.9, 1712.1)	330.5 (-116.0, 873.2)	714.8 (145.9, 1342.5)	1548.9 (556.3, 2589.3)	3500.4 (782.1, 6517.0)
WNC	Bayesian	50.4 (11.3, 91.2)	33.5 (-8.9, 80.2)	24.8 (5.2, 45.3)	30.6 (11.3, 49.7)	139.3 (18.9, 266.4)
	CMAQ	93.8 (20.7, 171.8)	61.0 (-15.9, 148.4)	45.3 (9.4, 83.2)	57.9 (21.3, 94.3)	258.0 (35.5, 497.7)

Figure 10: **Distribution of cumulative health burden by county.** For each county, we aggregated the number of hospitalizations for respiratory illness across all age groups related to fire-contributed $PM_{2.5}$ (the Bayesian estimate). The map displays the number of hospital admissions estimated over the 2008-2012 wildfire seasons.



6 Discussion

We present a novel potential outcomes framework that leverages numerical model output to estimate fire-contributed $PM_{2.5}$ while taking spatial correlation into account and modeling interference between sites. Using a Bayesian spatial downscaling model and monitoring data, we bias-correct CMAQ-estimated counterfactual outcomes for $PM_{2.5}$ under fire and no-fire regimes, and model correlation between potential outcomes. Assuming consistency between the potential outcomes and the observations based on a CMAQ-derived treatment indicator, and that confounding is accounted for conditional on CMAQ data, we show that the resulting estimate of fire-contributed $PM_{2.5}$ has a valid causal interpretation.

We provide a spatially-resolved estimate for fire-contributed $PM_{2.5}$ and uncertainty across the contiguous U.S. We found that the causal estimate of wildland fires on $PM_{2.5}$ reached the highest levels in the West, Northwest and Southeast regions. The western parts of the U.S. are impacted by large wildfires and frequent prescribed and agricultural burns are observed in the Southeast. The number of estimated hospitalizations due to exposure to fire-contributed $PM_{2.5}$ also reached a maximum in these regions, particularly in central California. Our estimates are lower than those produced by CMAQ. This particular application can be used by health professionals and environmental managers to better understand the health burden associated with fire events in their communities. Equipped with health burden estimates and uncertainty, they would be able to better anticipate the number of patients to expect and to plan accordingly. In this analysis, we estimated the number of cumulative respiratory hospitalizations per county; it is possible to compute other outcomes related to $PM_{2.5}$ exposure including all-cause mortality, cardiovascular outcomes, etc.

The study has limitations and strengths. We take a model-based approach that relies on relatively simple separable stationary Gaussian processes. Given the size of the data for this particular study, this approach is warranted, but could be revisited if used for smaller spatial regions. The approach is however generalizable to related research questions concerning how fire-contributed $PM_{2.5}$ depends on the specific features of wildland fires such as their location, strength, etc. or attribution of $PM_{2.5}$ to a single fire in which case CMAQ model would be run with corresponding forcings. These questions are critical in the environmental management context when it has to be shown that a specific fire caused exceedances of regulatory air quality standards. The proposed causal inference framework can also be generalized to wider range of attribution studies where potential outcomes can be represented using numerical modeling approaches e.g. in climate science, forestry, materials science, etc. In each case, the potential outcomes would differ by the factor of attribution whose impact is the objective of inference. Under the given assumptions and with bias correction we show that the resulting inference has a valid causal interpretation.

References

- Attribution of Extreme Weather Events in the Context of Climate Change. Technical report, National Academies of Sciences, Engineering, and Medicine, Washington, D.C., (2016).
- Allen, M. R. and Stott, P. A. (2003). Estimating signal amplitudes in optimal fingerprinting, Part I: Theory. *Climate Dynamics*, **21(5-6)**, 477–491.
- BenMAP. Technical report. Environmental Benefits Mapping and Analysis Program, Community Edition, User’s Manual Appendices, pages 34–44, (2017).
- Berrocal, V. J., Gelfand, A. E., and Holland, D. M. (2010). A spatio-temporal downscaler for output from numerical models. *Journal of Agricultural, Biological, and Environmental Statistics*, **15(2)**, 176–197.
- Chilès, J.-P. and Delfiner, P., (2012). *Geostatistics: Modeling Spatial Uncertainty*. Wiley Series in Probability and Statistics. John Wiley & Sons, Inc., Hoboken, NJ, USA.
- Cressie, N. A. C., (1993). *Statistics for Spatial Data*. Wiley Series in Probability and Statistics. John Wiley & Sons, Inc., Hoboken, NJ, USA.
- Delfino, R. J., Brummel, S., Wu, J., Stern, H., Ostro, B., Lipsett, M., Winer, A., Street, D. H., Zhang, L., Tjoa, T., and Gillen, D. L. (2009). The relationship of respiratory and cardiovascular hospital admissions to the southern California wildfires of 2003. *Occupational and Environmental Medicine*, **66(3)**, 189–197.
- Dennekamp, M. and Abramson, M. J. (2011). The effects of bushfire smoke on respiratory health. *Respirology*, **16(2)**, 198–209.
- Dennekamp, M., Straney, L. D., Erbas, B., Abramson, M. J., Keywood, M., Smith, K., Sim, M. R., Glass, D. C., Del Monaco, A., Haikerwal, A., and Tonkin, A. M. (2015). Forest fire smoke exposures and out-of-hospital cardiac arrests in Melbourne, Australia: A case-crossover study. *Environmental Health Perspectives*, **123(10)**, 959–964.

- Dominici, F., Greenstone, M., and Sunstein, C. R. (2014). Particulate Matter Matters. *Science*, **344**, 257–259.
- Fuentes, M. and Raftery, A. E. (2005). Model Evaluation and Spatial Interpolation by Bayesian Combination of Observations with Outputs from Numerical Models. *Biometrics*, **61(1)**, 36–45.
- Gelfand, A. E., Kim, H.-J., Sirmans, C. F., and Banerjee, S. (2003). Spatial Modeling with Spatially Varying Coefficient Processes. *Source Journal of the American Statistical Association*, **98(462)**, 387–396.
- Gelfand, A. E., Schmidt, A. M., Banerjee, S., and Sirmans, C. F. (2004). Nonstationary Multivariate Process Modeling through Spatially Varying Coregionalization. *Test*, **13(2)**, 263–312.
- Haikerwal, A., Akram, M., Del Monaco, A., Smith, K., Sim, M. R., Meyer, M., Tonkin, A. M., Abramson, M. J., and Dennekamp, M. (2015). Impact of Fine Particulate Matter (PM_{2.5}) Exposure During Wildfires on Cardiovascular Health Outcomes. *Journal of the American Heart Association*, **4(7)**, e001653.
- Haikerwal, A., Akram, M., Sim, M. R., Meyer, M., Abramson, M. J., and Dennekamp, M. (2016). Fine particulate matter (PM_{2.5}) exposure during a prolonged wildfire period and emergency department visits for asthma. *Respirology*, **21(1)**, 88–94.
- Halloran, M. E. and Struchiner, C. J. (1991). Study designs for dependent happenings. *Epidemiology*, **2(5)**, 331–8.
- Hannart, A., Pearl, J., Otto, F. E. L., Naveau, P., and Ghil, M. (2015). Causal counterfactual theory for the attribution of weather and climate-related events. *Bulletin of the American Meteorological Society*, **97**, 99–110.
- Hansen, B. B. (2008). The prognostic analogue of the propensity score. *Biometrika*, **95**, 481–488.

- Hegerl, G. and Zwiers, F. (2011). Use of models in detection and attribution of climate change. *Wiley Interdisciplinary Reviews: Climate Change*, **2(4)**, 570–591.
- Hernán, M. A., Alonso, A., Logan, R., Grodstein, F., Michels, K. B., Willett, W. C., Manson, J. E., and Robins, J. M. (2008). Observational Studies Analyzed Like Randomized Experiments. *Epidemiology*, **19(6)**, 766–779.
- Holland, P. W. (1986). Statistics and Causal Inference: Rejoinder. *Journal of the American Statistical Association*, **81(396)**, 968–970.
- Hong, G. and Raudenbush, S. W. (2006). Evaluating Kindergarten Retention Policy. *Journal of the American Statistical Association*, **101(475)**, 901–910.
- Hudgens, M. G. and Halloran, M. E. (2008). Toward Causal Inference With Interference. *Journal of the American Statistical Association*, **103(482)**, 832–842.
- Johnston, F. H., Henderson, S. B., Chen, Y., Randerson, J. T., Marlier, M., DeFries, R. S., Kinney, P., Bowman, D. M. J. S., and Brauer, M. (2012). Estimated global mortality attributable to smoke from landscape fires. *Environmental Health Perspectives*, **120(5)**, 695–701.
- Kao, E. K. (2017). Causal inference under network interference: A framework for experiments on social networks. *arXiv preprint arXiv:1708.08522*.
- Katzfuss, M., Hammerling, D., and Smith, R. L. (2017). A Bayesian hierarchical model for climate change detection and attribution. *Geophysical Research Letters*, **44(11)**, 5720–5728.
- Kennedy, M. C. and O’Hagan, A. (2001). Bayesian calibration of computer models. *Journal of the Royal Statistical Society: Series B (Statistical Methodology)*, **63(3)**, 425–464.
- Knutson, T., Kossin, J., Mears, C., Perlwitz, J., and Wehner, M., (2017). Detection and attribution of climate change. In *Climate Science Special Report: Fourth National*

- Climate Assessment, Volume I*, pages 114–132. U.S. Global Change Research Program, Washington, DC, USA.
- McKenzie, D., Shankar, U., Keane, R. E., Stavros, E. N., Heilman, W. E., Fox, D. G., and Riebau, A. C. (2014). Earth’s Future Smoke consequences of new wildfire regimes driven by climate change. *Earth’s Future*, **2(2)**, 35–59.
- Rappold, A. G., Stone, S. L., Cascio, W. E., Neas, L. M., Kilaru, V. J., Carraway, M. S., Szykman, J. J., Ising, A., Cleve, W. E., Meredith, J. T., Vaughan-Batten, H., Deyneka, L., and Devlin, R. B. (2011). Peat bog wildfire smoke exposure in rural North Carolina is associated with cardiopulmonary emergency department visits assessed through syndromic surveillance. *Environmental Health Perspectives*, **119(10)**, 1415–1420.
- Rappold, A. G., Reyes, J., Pouliot, G., Cascio, W. E., and Diaz-Sanchez, D. (2017). Community Vulnerability to Health Impacts of Wildland Fire Smoke Exposure. *Environmental Science & Technology*, **51(12)**, 6674–6682.
- Rosenbaum, P. R. (2007). Interference Between Units in Randomized Experiments. *Journal of the American Statistical Association*, **102(477)**, 191–200.
- Rubin, D. B. (1978). Bayesian Inference for Causal Effects: The Role of Randomization. *The Annals of Statistics*, **6(1)**, 34–58.
- Schmidt, A. M. and Gelfand, A. E. (2003). A Bayesian coregionalization approach for multivariate pollutant data. *Journal of Geophysical Research: Atmospheres*, **108(D24)**.
- Sobel, M. E. (2006). What Do Randomized Studies of Housing Mobility Demonstrate? *Journal of the American Statistical Association*, **101(476)**, 1398–1407.
- Stavros, E. N., Mckenzie, D., and Larkin, N. (2014). The climate-wildfire-air quality system: Interactions and feedbacks across spatial and temporal scales. *Wiley Interdisciplinary Reviews: Climate Change*, **5(6)**, 719–733.

- Tchetgen, E. J. T. and VanderWeele, T. J. (2012). On causal inference in the presence of interference. *Statistical Methods in Medical Research*, **21(1)**, 55–75.
- US Environmental Protection Agency. AirData Download Files Documentation, (2015).
- U.S. EPA. (2009). Integrated science assessment for particulate matter. *US Environmental Protection Agency: Washington DC, USA*.
- US EPA. (2018). Particulate Matter (PM2.5) Trends.
- U.S. EPA. Overview of science processes in CMAQ, (2019). URL <https://www.epa.gov/cmaq/overview-science-processes-cmaq>.
- U.S. Forest Service. AirFire research team, (2019). URL <https://sites.google.com/firenet.gov/wfaqrp-external/smoke-modeling>.
- Wettstein, Z. S., Hoshiko, S., Fahimi, J., Harrison, R. J., Cascio, W. E., and Rappold, A. G. (2018). Cardiovascular and Cerebrovascular Emergency Department Visits Associated With Wildfire Smoke Exposure in California in 2015. *Journal of the American Heart Association*, **7(8)**, e007492.
- Zigler, C. M., Dominici, F., and Wang, Y. (2012). Estimating causal effects of air quality regulations using principal stratification for spatially correlated multivariate intermediate outcomes. *Biostatistics*, **13(2)**, 289–302.
- Zigler, C. M., Choirat, C., and Dominici, F. (2017). Impact of National Ambient Air Quality Standards nonattainment designations on particulate pollution and health. *Epidemiology*, **29(2)**, 165–174.

Acknowledgements

This work was partially supported by grants from the National Institutes of Health (R01ES027892, R01DE024984-01A1), the National Science Foundation (DMS-1513579 and DMS-1811245),

the National Cancer Institute (P01CA142538), the Department of the Interior (14-1-04-9) and Oak Ridge Associated Universities.

Appendix A Proof of Theorem 1

Proof. To relate the potential outcome processes to the induced model of the observed outcome process, consider $Y_t^{\text{miss}}(\mathbf{s})$ as the observation of the potential outcome that is missing under each regime, i.e.,

$$Y_t(\mathbf{s}, 0) = \begin{cases} Y_t(\mathbf{s}) & \text{if } C_t(\mathbf{s}) = 0 \\ Y_t^{\text{miss}}(\mathbf{s}) & \text{if } C_t(\mathbf{s}) = 1 \end{cases} \quad \text{and} \quad Y_t(\mathbf{s}, 1) = \begin{cases} Y_t^{\text{miss}}(\mathbf{s}) & \text{if } C_t(\mathbf{s}) = 0 \\ Y_t(\mathbf{s}) & \text{if } C_t(\mathbf{s}) = 1. \end{cases}$$

Hence, the joint distribution of the potential outcomes, $Y_t(\mathbf{s}, 0)$ and $Y_t(\mathbf{s}, 1)$, is the joint distribution of the observed and missing observations $Y_t(\mathbf{s})$ and $Y_t^{\text{miss}}(\mathbf{s})$.

Denoting Θ as all parameters in the potential outcomes model, the likelihood function of Θ is

$$\begin{aligned} & \prod_{t=1}^T \int f(\mathbf{Y}_t, \mathbf{Y}_t^{\text{miss}} | \hat{\boldsymbol{\theta}}_t, \hat{\boldsymbol{\delta}}_t, \Theta) d\mathbf{Y}_t^{\text{miss}} \\ &= \prod_{t=1}^T \int f(\mathbf{Y}_t, \mathbf{Y}_t^{\text{miss}} | \hat{\boldsymbol{\theta}}_t, \hat{\boldsymbol{\delta}}_t, \mathbf{C}_t, \Theta) d\mathbf{Y}_t^{\text{miss}} \\ &= \prod_{t=1}^T \left[\int f(\mathbf{Y}_t^{\text{miss}} | \mathbf{Y}_t, \hat{\boldsymbol{\theta}}_t, \hat{\boldsymbol{\delta}}_t, \mathbf{C}_t, \Theta) d\mathbf{Y}_t^{\text{miss}} \right] f(\mathbf{Y}_t | \hat{\boldsymbol{\theta}}_t, \hat{\boldsymbol{\delta}}_t, \mathbf{C}_t, \Theta) \\ &= \prod_{t=1}^T f(\mathbf{Y}_t | \hat{\boldsymbol{\theta}}_t, \hat{\boldsymbol{\delta}}_t, \mathbf{C}_t, \Theta), \end{aligned} \tag{6}$$

where the second line follows by Assumption 1. By (6), Θ depends only on the observed processes, which completes the proof. \square

Appendix B Bayesian Analysis and Computing

We conduct our analysis using a Bayesian framework, placing prior distributions on all model parameters. At the first level, we have observations $\mathbf{Y}_t = (Y_t(\mathbf{s}_1), \dots, Y_t(\mathbf{s}_n))^T$ denoting measured PM_{2.5} measured on day t , $t = 1, \dots, m$, for n sites, $\mathbf{s}_1, \dots, \mathbf{s}_n$, modeled as multivariate normal:

$$\mathbf{Y}_1, \dots, \mathbf{Y}_m \stackrel{indp}{\sim} MVN(\boldsymbol{\theta}_t + \mathbf{C}_t \boldsymbol{\delta}_t, \sigma^2 I_n),$$

where $\boldsymbol{\theta}_t$ and $\boldsymbol{\delta}_t$ are n -vectors of the true background and fire-contributed PM_{2.5} processes on day t , respectively, \mathbf{C}_t is an $n \times n$ diagonal matrix with binary entries, $C_t(\mathbf{s})$, that indicate fire impacts at all sites on day t and σ^2 is error variance. We place a non-informative inverse-gamma prior on σ^2 : $\sigma^2 \sim IG(0.1, 0.1)$.

We assume the priors for the true PM_{2.5} spatial processes follow a bivariate Gaussian process for $t = 1, \dots, m$:

$$\begin{pmatrix} \boldsymbol{\theta}_t \\ \boldsymbol{\delta}_t \end{pmatrix} \sim \mathcal{GP} \left(\begin{bmatrix} B_0(\hat{\boldsymbol{\theta}}_t) \\ B_1(\hat{\boldsymbol{\delta}}_t) \end{bmatrix}, \begin{bmatrix} \sigma_1^2 & \sigma_{12} \\ \sigma_{12} & \sigma_2^2 \end{bmatrix} \otimes C(\phi_1) \right) \quad (7)$$

where $\hat{\boldsymbol{\theta}}_t$ and $\hat{\boldsymbol{\delta}}_t$ are the numerical model output on (background) and wildfire-contributed PM_{2.5} for all sites on day t , respectively. The mean functions are $B_0(\boldsymbol{\theta}_t) = \boldsymbol{\alpha}_0 + \boldsymbol{\beta}_0 \hat{\boldsymbol{\theta}}_t$ and $B_1(\boldsymbol{\delta}_t) = \boldsymbol{\alpha}_1 + \boldsymbol{\beta}_1 \hat{\boldsymbol{\delta}}_t$, where $\boldsymbol{\alpha}_0$ and $\boldsymbol{\alpha}_1$ are n -vectors of additive bias for sites $\mathbf{s}_1, \dots, \mathbf{s}_n$, and $\boldsymbol{\beta}_0$ and $\boldsymbol{\beta}_1$ are n -vectors of multiplicative bias for sites $\mathbf{s}_1, \dots, \mathbf{s}_n$. The $n \times n$ matrix, $C(\phi_1)$, is an exponential decay correlation matrix such that $C_{i,j} = \exp(-\|\mathbf{s}_i - \mathbf{s}_j\|/\phi_1)$ for two sites, \mathbf{s}_i and \mathbf{s}_j . Also, the covariance parameter can be written as $\sigma_{12} = \sigma_1 \sigma_2 \gamma$.

We re-parameterize the model in (7) as a linear model of co-regionalization (Gelfand et al., 2004) for ease of computation. Define $s_1^2 = \sigma_1^2$, $\rho = \frac{\sigma_{12}}{\sigma_1^2}$ and $s_2^2 = \sigma_2^2 - \frac{\sigma_{12}^2}{\sigma_1^2}$. Then we have

$$\begin{aligned} \boldsymbol{\theta}_t &\sim \mathcal{GP} \left(B_0(\hat{\boldsymbol{\theta}}_t), s_1^2 C(\phi_1) \right) \\ \boldsymbol{\delta}_t | \boldsymbol{\theta}_t &\sim \mathcal{GP} \left(B_1(\hat{\boldsymbol{\delta}}_t) + \rho(\boldsymbol{\theta}_t - B_0(\hat{\boldsymbol{\theta}}_t)), s_2^2 C(\phi_1) \right) \end{aligned}$$

We assign noninformative priors to the covariance parameters: $s_1^2 \sim IG(0.1, 0.1)$, $s_2^2 \sim IG(0.1, 0.1)$, $\rho \sim N(0, 100)$. To get posterior means of σ_1^2 , σ_2^2 , σ_{12} and the correlation parameter, γ ,

$$\hat{\sigma}_1^2 = \hat{s}_1^2, \quad \hat{\sigma}_{12} = \hat{\rho}\hat{s}_1^2, \quad \hat{\sigma}_2^2 = \hat{\rho}^2\hat{s}_1^2 + \hat{s}_2^2$$

and since $\gamma = \frac{\sigma_{12}}{\sigma_1\sigma_2}$,

$$\hat{\gamma} = \frac{\hat{\rho}\hat{s}_1}{\sqrt{\hat{\rho}^2\hat{s}_1^2 + \hat{s}_2^2}}.$$

We let the priors of the bias terms vary spatially with constant mean:

$$\begin{aligned} \boldsymbol{\alpha}_0 &\sim MVN(\mu_{\alpha_0}\mathbf{1}_n, \sigma_{\alpha_0}^2 C(\phi_2)) \\ \boldsymbol{\beta}_0 &\sim MVN(\mu_{\beta_0}\mathbf{1}_n, \sigma_{\beta_0}^2 C(\phi_2)) \\ \boldsymbol{\alpha}_1 &\sim MVN(\mu_{\alpha_1}\mathbf{1}_n, \sigma_{\alpha_1}^2 C(\phi_2)) \\ \boldsymbol{\beta}_1 &\sim MVN(\mu_{\beta_1}\mathbf{1}_n, \sigma_{\beta_1}^2 C(\phi_2)). \end{aligned}$$

We assign non-informative priors to the hyper-parameters:

$$\begin{aligned} \mu_{\alpha_0}, \mu_{\beta_0}, \mu_{\alpha_1}, \mu_{\beta_1} &\sim N(0, 100^2) \\ \sigma_{\alpha_0}^2, \sigma_{\beta_0}^2, \sigma_{\alpha_1}^2, \sigma_{\beta_1}^2 &\sim IG(0.1, 0.1) \\ \log(\phi_2) &\sim N(0, 500). \end{aligned}$$

B.1 Derivation of Full Conditionals

Most of the parameter models have conditionally conjugate priors and are thus updated using Gibbs sampling. Below we give the full conditional distribution for these parameters:

$$\boldsymbol{\theta}_t | \mathbf{Y}_t \sim \mathcal{N} \left((\Sigma_y^{-1} + \Sigma_\theta^{-1} + \rho^2 \Sigma_\delta^{-1})^{-1} (\Sigma_y^{-1} (\mathbf{Y}_t - C_t \boldsymbol{\delta}_t) + \Sigma_\theta^{-1} B_0(\hat{\boldsymbol{\theta}}_t) + \rho \Sigma_\delta^{-1} (\boldsymbol{\delta}_t - B_1(\hat{\boldsymbol{\delta}}_t) + \rho B_0(\hat{\boldsymbol{\theta}}_t))), \right. \\ \left. (\Sigma_y^{-1} + \Sigma_\theta^{-1} + \rho^2 \Sigma_\delta^{-1})^{-1} \right)$$

$$\boldsymbol{\delta}_t | \mathbf{Y}_t \sim \mathcal{N} \left((C_t^T \Sigma_y^{-1} C_t + \Sigma_\delta^{-1})^{-1} (C_t^T \Sigma_y^{-1} (\mathbf{Y}_t - \boldsymbol{\theta}_t) + \Sigma_\delta^{-1} (B_1(\hat{\boldsymbol{\delta}}_t) + \rho(\boldsymbol{\theta}_t - B_0(\hat{\boldsymbol{\theta}}_t)))), \right. \\ \left. (C_t^T \Sigma_y^{-1} C_t + \Sigma_\delta^{-1})^{-1} \right)$$

$$\sigma^2 | \mathbf{Y}_t \sim \mathcal{IG} \left(\frac{nm}{2} + 0.1, \left(\frac{1}{2} \sum_{t=1}^m (\mathbf{Y}_t - (\boldsymbol{\theta}_t + C_t \boldsymbol{\delta}_t))^T (\mathbf{Y}_t - (\boldsymbol{\theta}_t + C_t \boldsymbol{\delta}_t)) \right) + 0.1 \right)$$

$$\boldsymbol{\alpha}_0 | \mathbf{Y}_t, \boldsymbol{\theta}_t, \boldsymbol{\delta}_t \sim \mathcal{N} \left((m \Sigma_\theta^{-1} + m \rho^2 \Sigma_\delta^{-1} + \Sigma_{\alpha_0}^{-1})^{-1} \left(\sum_{t=1}^m \Sigma_\theta^{-1} (\boldsymbol{\theta}_t - \hat{\boldsymbol{\theta}}_t \boldsymbol{\beta}_0) + \rho \Sigma_\delta^{-1} (\rho(\boldsymbol{\theta}_t - \hat{\boldsymbol{\theta}}_t \boldsymbol{\beta}_0) - \right. \right. \\ \left. \left. (\boldsymbol{\delta}_t - B_1(\hat{\boldsymbol{\delta}}_t))) + \mu_{\alpha_0} \Sigma_{\alpha_0}^{-1} \mathbf{1}_n \right), (m \Sigma_\theta^{-1} + m \rho^2 \Sigma_\delta^{-1} + \Sigma_{\alpha_0}^{-1})^{-1} \right)$$

$$\boldsymbol{\beta}_0 | \mathbf{Y}_t, \boldsymbol{\theta}_t, \boldsymbol{\delta}_t \sim \mathcal{N} \left(\left(\sum_{t=1}^m \hat{\boldsymbol{\theta}}_t^T (\Sigma_\theta^{-1} + \rho^2 \Sigma_\delta^{-1}) \hat{\boldsymbol{\theta}}_t + \Sigma_{\beta_0}^{-1} \right)^{-1} \left(\sum_{t=1}^m \hat{\boldsymbol{\theta}}_t^T \Sigma_\theta^{-1} (\boldsymbol{\theta}_t - \boldsymbol{\alpha}_0) + \rho \hat{\boldsymbol{\theta}}_t^T \Sigma_\delta^{-1} (\rho(\boldsymbol{\theta}_t - \boldsymbol{\alpha}_0) - \right. \right. \\ \left. \left. (\boldsymbol{\delta}_t - B_1(\hat{\boldsymbol{\delta}}_t))) + \mu_{\beta_0} \Sigma_{\beta_0}^{-1} \mathbf{1}_n \right), \left(\sum_{t=1}^m \hat{\boldsymbol{\theta}}_t^T (\Sigma_\theta^{-1} + \rho^2 \Sigma_\delta^{-1}) \hat{\boldsymbol{\theta}}_t + \Sigma_{\beta_0}^{-1} \right)^{-1} \right)$$

$$\boldsymbol{\alpha}_1 | \mathbf{Y}_t, \boldsymbol{\theta}_t, \boldsymbol{\delta}_t \sim \mathcal{N} \left((m \Sigma_\delta^{-1} + \Sigma_{\alpha_1}^{-1})^{-1} \left(\sum_{t=1}^m \Sigma_\delta^{-1} (\boldsymbol{\delta}_t - (\hat{\boldsymbol{\delta}}_t \boldsymbol{\beta}_1 + \rho(\boldsymbol{\theta}_t - B_0(\hat{\boldsymbol{\theta}}_t)))) + \mu_{\alpha_1} \Sigma_{\alpha_1}^{-1} \mathbf{1}_n \right), \right. \\ \left. (m \Sigma_\delta^{-1} + \Sigma_{\alpha_1}^{-1})^{-1} \right)$$

$$\boldsymbol{\beta}_1 | \mathbf{Y}_t, \boldsymbol{\theta}_t, \boldsymbol{\delta}_t \sim \mathcal{N} \left(\left(\sum_{t=1}^m \hat{\boldsymbol{\delta}}_t^T \Sigma_\delta^{-1} \hat{\boldsymbol{\delta}}_t + \Sigma_{\beta_1}^{-1} \right)^{-1} \left(\sum_{t=1}^m \hat{\boldsymbol{\delta}}_t^T \Sigma_\delta^{-1} (\boldsymbol{\delta}_t - \boldsymbol{\alpha}_1 - \rho(\boldsymbol{\theta}_t - B_0(\hat{\boldsymbol{\theta}}_t))) + \mu_{\beta_1} \Sigma_{\beta_1}^{-1} \mathbf{1}_n \right), \right. \\ \left. \left(\sum_{t=1}^m \hat{\boldsymbol{\delta}}_t^T \Sigma_\delta^{-1} \hat{\boldsymbol{\delta}}_t + \Sigma_{\beta_1}^{-1} \right)^{-1} \right)$$

$$\rho | \mathbf{Y}_t, \boldsymbol{\theta}_t, \boldsymbol{\delta}_t \sim \mathcal{N} \left(\left(\frac{1}{100} + \sum_{t=1}^m (\boldsymbol{\theta}_t - B_0(\hat{\boldsymbol{\theta}}_t))^T \Sigma_{\delta}^{-1} (\boldsymbol{\theta}_t - B_0(\hat{\boldsymbol{\theta}}_t)) \right)^{-1} \sum_{t=1}^m (\boldsymbol{\delta}_t - B_1(\hat{\boldsymbol{\delta}}_t))^T \Sigma_{\delta}^{-1} (\boldsymbol{\delta}_t - B_1(\hat{\boldsymbol{\delta}}_t)), \right. \\ \left. \left(\frac{1}{100} + \sum_{t=1}^m (\boldsymbol{\theta}_t - B_0(\hat{\boldsymbol{\theta}}_t))^T \Sigma_{\delta}^{-1} (\boldsymbol{\theta}_t - B_0(\hat{\boldsymbol{\theta}}_t)) \right)^{-1} \right)$$

$$s_1^2 | \mathbf{Y}_t, \boldsymbol{\theta}_t \sim \mathcal{IG} \left(\frac{nm}{2} + 0.1, \left(\frac{1}{2} \sum_{t=1}^m (\boldsymbol{\theta}_t - B_0(\hat{\boldsymbol{\theta}}_t))^T C(\phi_1)^{-1} (\boldsymbol{\theta}_t - B_0(\hat{\boldsymbol{\theta}}_t)) + 0.1 \right) \right)$$

$$s_2^2 | \mathbf{Y}_t, \boldsymbol{\delta}_t \sim \mathcal{IG} \left(\frac{nm}{2} + 0.1, \left(\frac{1}{2} \sum_{t=1}^m (\boldsymbol{\delta}_t - (B_1(\hat{\boldsymbol{\delta}}_t) + \rho (\boldsymbol{\theta}_t - B_0(\hat{\boldsymbol{\theta}}_t))))^T C(\phi_1)^{-1} (\boldsymbol{\delta}_t - (B_1(\hat{\boldsymbol{\delta}}_t) + \rho (\boldsymbol{\theta}_t - B_0(\hat{\boldsymbol{\theta}}_t)))) + 0.1 \right) \right)$$

$$\mu_{\alpha_i} | \mathbf{Y}_t \sim \mathcal{N} \left(\left(\mathbf{1}_n^T \Sigma_{\alpha_i}^{-1} \mathbf{1}_n + \frac{1}{100^2} \right)^{-1} \mathbf{1}_n^T \Sigma_{\alpha_i}^{-1} \boldsymbol{\alpha}_i, \left(\mathbf{1}_n^T \Sigma_{\alpha_i}^{-1} \mathbf{1}_n + \frac{1}{100^2} \right)^{-1} \right)$$

$$\mu_{\beta_i} | \mathbf{Y}_t \sim \mathcal{N} \left(\left(\mathbf{1}_n^T \Sigma_{\beta_i}^{-1} \mathbf{1}_n + \frac{1}{100^2} \right)^{-1} \mathbf{1}_n^T \Sigma_{\beta_i}^{-1} \boldsymbol{\beta}_i, \left(\mathbf{1}_n^T \Sigma_{\beta_i}^{-1} \mathbf{1}_n + \frac{1}{100^2} \right)^{-1} \right)$$

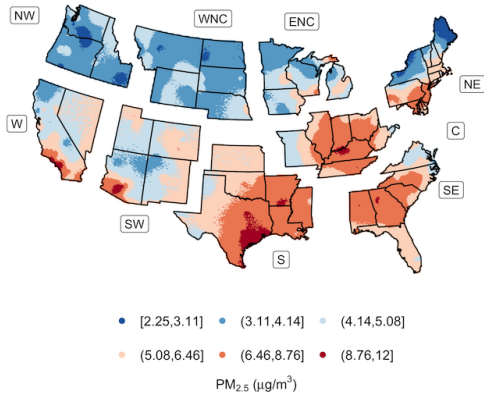
$$\sigma_{\alpha_i}^2 | \mathbf{Y}_t \sim \mathcal{IG} \left(\frac{n}{2} + 0.1, \frac{1}{2} (\boldsymbol{\alpha}_i - \mu_{\alpha_i} \mathbf{1}_n)^T C(\phi_2)^{-1} (\boldsymbol{\alpha}_i - \mu_{\alpha_i} \mathbf{1}_n) + 0.1 \right)$$

$$\sigma_{\beta_i}^2 | \mathbf{Y}_t \sim \mathcal{IG} \left(\frac{n}{2} + 0.1, \frac{1}{2} (\boldsymbol{\beta}_i - \mu_{\beta_i} \mathbf{1}_n)^T C(\phi_2)^{-1} (\boldsymbol{\beta}_i - \mu_{\beta_i} \mathbf{1}_n) + 0.1 \right)$$

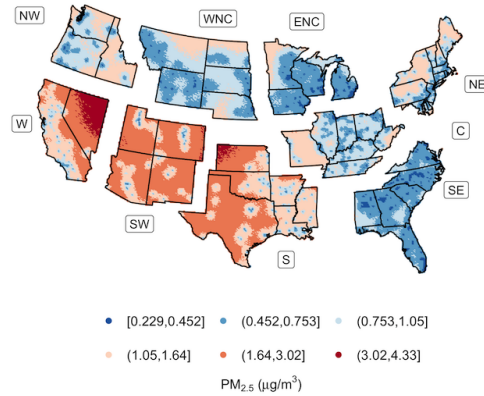
The range parameters, ϕ_1 and ϕ_2 are estimated empirically using variograms.

B.2 Effect Estimates

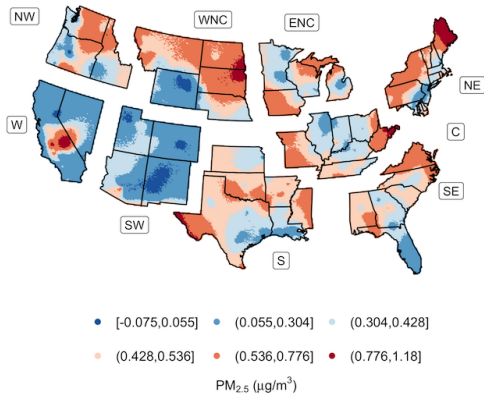
Figure 11: **Bias estimates for CMAQ's background $PM_{2.5}$.** The posterior mean standard deviation (SD) for additive bias (a,b) and multiplicative bias (c, d).



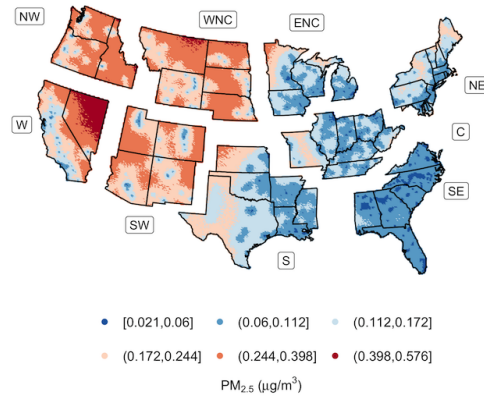
(a) Posterior Mean of $\alpha_0(s)$ ($\mu g/m^3$)



(b) Posterior SD of $\alpha_0(s)$ ($\mu g/m^3$)

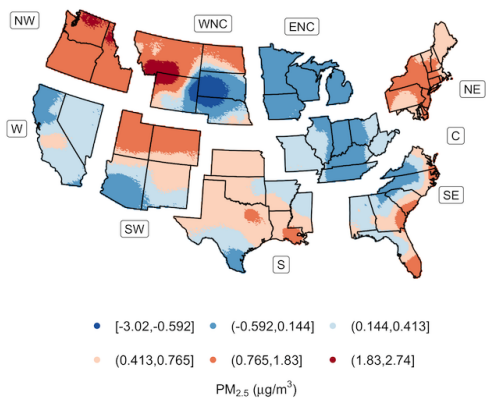


(c) Posterior Mean of $\beta_0(s)$ ($\mu g/m^3$)

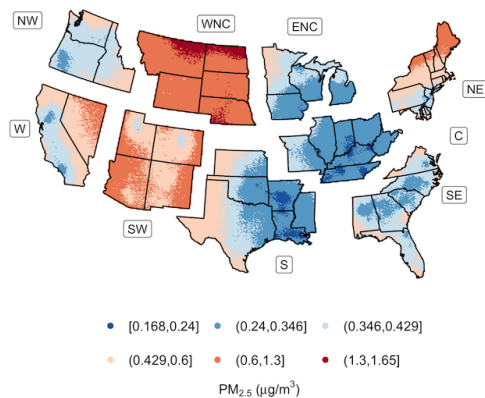


(d) Posterior SD of $\beta_0(s)$ ($\mu g/m^3$)

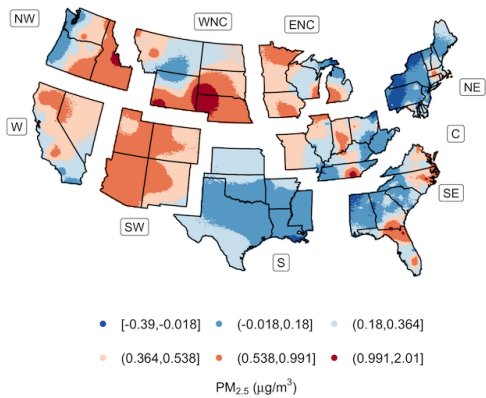
Figure 12: **Bias estimates for CMAQ’s fire-contributed $PM_{2.5}$.** The posterior mean standard deviation (SD) for additive bias (a,b) and multiplicative bias (c, d).



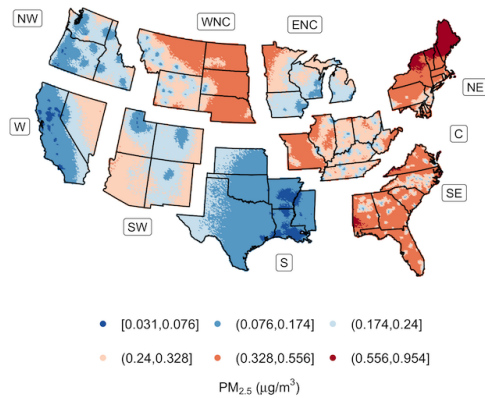
(a) Posterior Mean of $\alpha_1(s)$ ($\mu g/m^3$)



(b) Posterior SD of $\alpha_1(s)$ ($\mu g/m^3$)

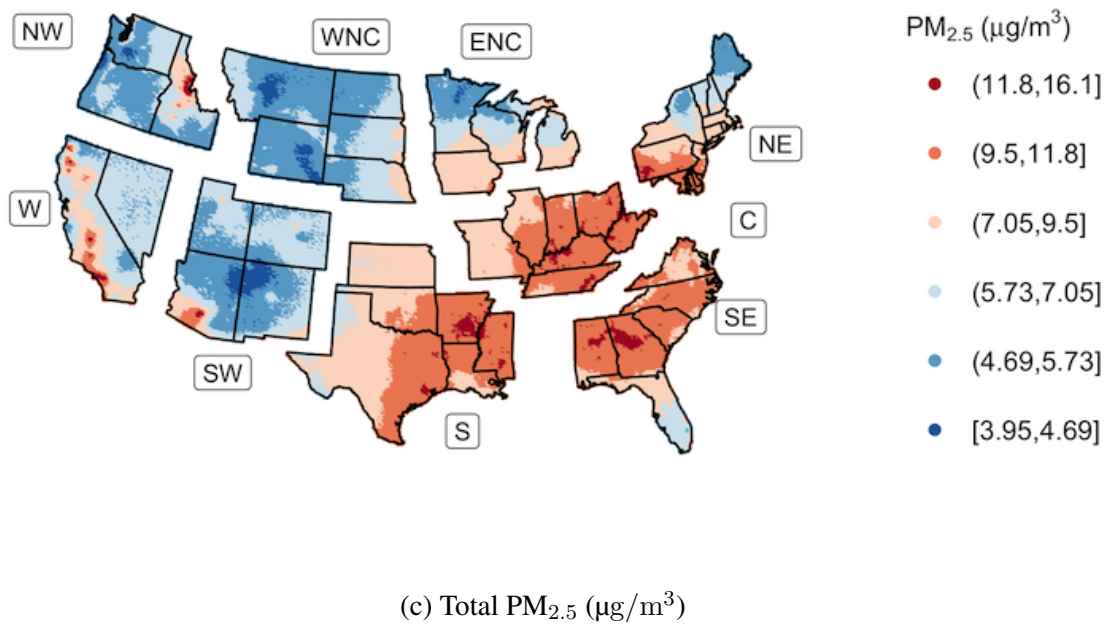
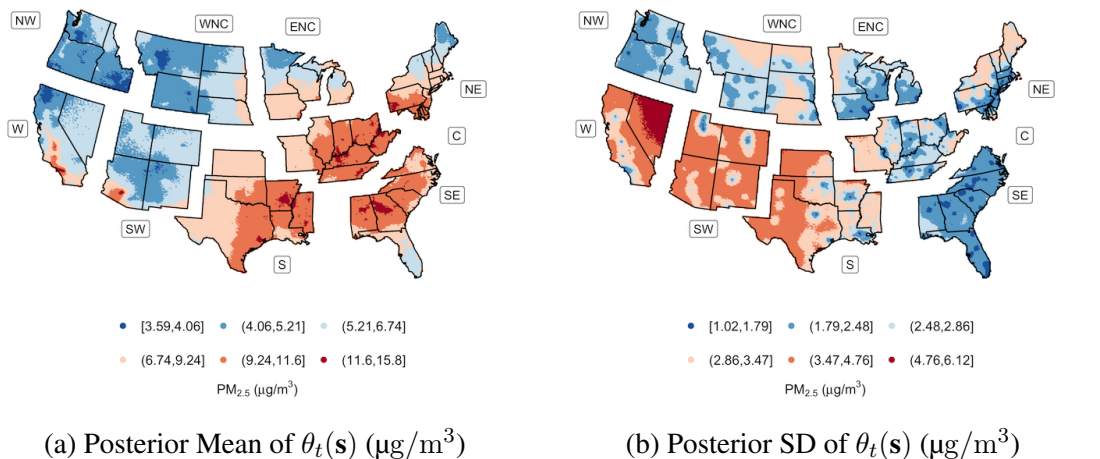


(c) Posterior Mean of $\beta_1(s)$ ($\mu g/m^3$)



(d) Posterior SD of $\beta_1(s)$ ($\mu g/m^3$)

Figure 13: Estimates from the Bayesian model of background $PM_{2.5}$. The posterior means (a) and associated standard deviation (b), as well as estimated total $PM_{2.5}$ (c).



B.3 Health Burden Analysis

Table 2: Age groups and relative rates (r_a) used to calculate health burden impact.

U.S. Census July 2010	Age Group (years)		Wildfire Period Relative Rate of Respiratory Hospitalization*
	Delfino et al. 2009	BenMaps/Our Analysis	
0-4	0-4	0-1	1.045
5-9, 10-14, 15-19	5-19	2-17	1.027
20-24		18-24	
25-29, 30-34		25-34	
35-39, 40-44	20-64	35-44	1.024
45-49, 50-54		45-54	
55-59, 60-64		55-64	
65-69, 70-74	65 and older	65-74	1.030
75-79, 80-84		75-84	
85 and older		85-99	

*Delfino et. al 2009

A spatial causal analysis of wildland fire-contributed $PM_{2.5}$ using numerical model output

Supplemental Materials

1 MCMC Convergence Diagnostics

MCMC convergence was assessed by visual examination of trace-plots and by calculating the effective sample sizes (ESS), displayed in this section for the most fire-prone and therefore most representative area, the West region. In Figure 1, we show the ESS and trace-plots for the causal effect estimate at ten randomly selected monitoring sites. The average ESS for the causal effect over all 96 of the monitoring sites was 281.09 (SD=139.649). This was calculated after a burn-in period of 5,000 iterations from 30,000 total iterations; trimming was not included. We also calculated the ESS of the causal effect at the CMAQ centroids (i.e. the Kriging points) was 1,089.7 (SD=950.5). This was computed after a burn-in period of 5,000 iterations; trimming was not included. The ESS for the causal effect estimate at each CMAQ centroid is displayed in Figure 2.

Figure 1: **Trace-plots and effective sample size for the causal effect estimates.** To monitor MCMC convergence, we visually examined trace-plots and computed the effective sample size (ESS). These plots show the effective sample sizes and trace-plots for the causal effect estimates at ten randomly selected monitoring sites (s) out of the 96 total sites the West Region.

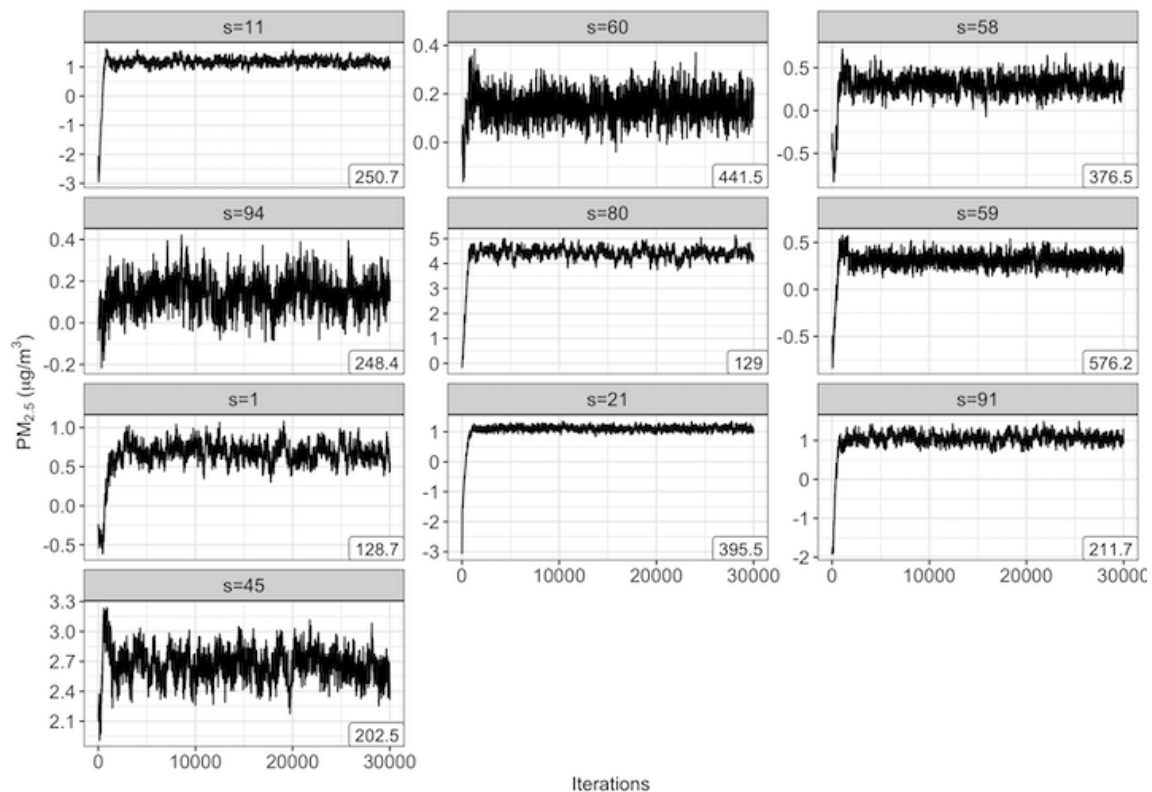
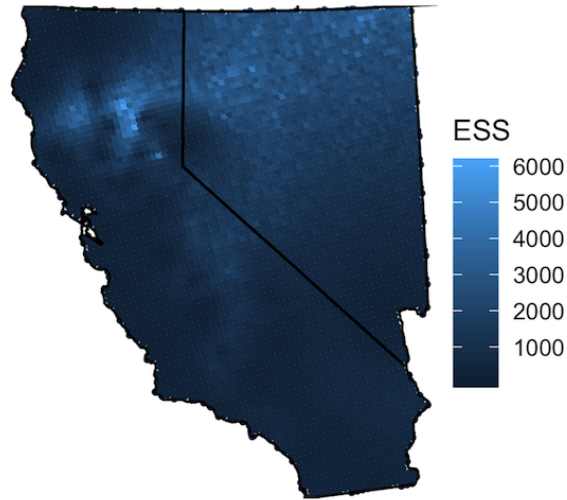


Figure 2: **Effective sample sizes for the causal effect estimate at the CMAQ centroids.** To monitor MCMC convergence, we computed the effective sample size (ESS) for the causal effect estimates in the West Region. This map shows the effective sample sizes at each CMAQ centroid.



2 Sensitivity to Regional Blocking

We conducted separate analyses for each region of the contiguous U.S. included in our study in order to run our analysis in parallel, thereby speeding up computation. A potential downside of this approach is that correlation between neighboring regions is ignored. Here, we demonstrate that ignoring this correlation has only a small impact.

We conducted a sensitivity test to determine the effects of running separate regional analyses that entailed running the analysis for the Northwest and Western regions as one and compared the resulting causal effect estimates to those from each region run with separate analyses. We chose to focus on the West and Northwest regions since the western US is the most prone to fires. In Figure 3, we display the estimated posterior means and standard deviations of the causal effects for the Northwest and Western regions as one and separately. The resulting spatial patterns are similar, leading us to conclude that our

analysis is robust to regional blocking.

3 Spatial Covariance Function

Here, we demonstrate the strength of the correlation between sites. We evaluate

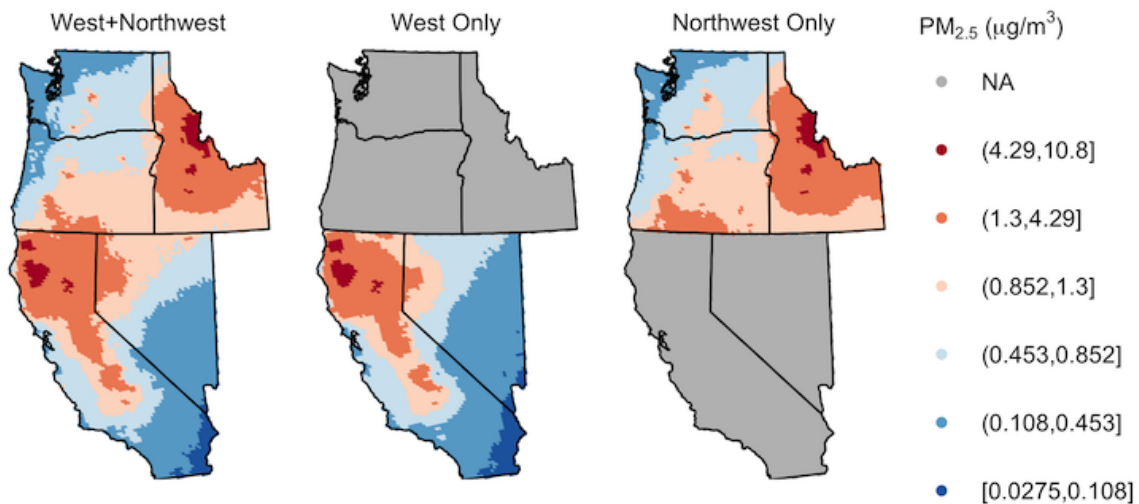
$$\text{Cov}[Y_t(\mathbf{s}), Y_t(\mathbf{s}') | \hat{\theta}_t(\mathbf{s}), \hat{\delta}_t(\mathbf{s})]$$

as defined in Equation (5) in the text, at the posterior mean of the model parameters for each combination of $(C_t(\mathbf{s}), C_t(\mathbf{s}'))$. Figure 4 displays the plotted covariance functions for each region. The black curve denotes the covariance for observations where neither site is co-located with smoke, the red curve is the covariance for sites where only one is co-located with smoke, and the green curves denote the covariance for two sites co-located with smoke. The strength of the covariance between observations varies between all of the regions, and is strongest in those regularly impacted with wildfire smoke (e.g. West, West North Central).

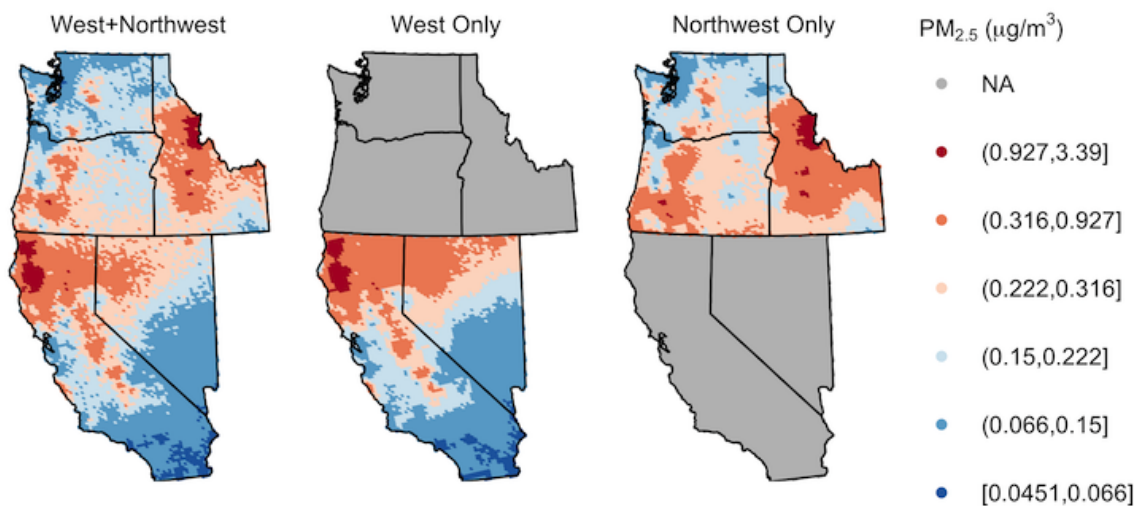
4 Sensitivity to τ

In this section, we provide sensitivity analysis to the choice of τ , the smoke presence threshold. In Table 1, we provide results from a cross-validation analysis and in Figure 5 we provide plots of the causal effect estimated under different values of τ to demonstrate robustness to choice of τ .

Figure 3: **Causal effect estimate for the West and Northwest regions separately versus combined.** Posterior means (top) and standard deviations (bottom) of the causal effect for the West and Northwest regions as one and separately. We present the 2nd, 25th, 50th, 75th, and 98th percentiles of the means and standard deviations.



(a) Posterior Mean



(b) Posterior Standard Deviation

Figure 4: **Spatial covariance functions.** The covariance functions from Equation (5) in the text evaluated at the posterior means of the model parameters for each combination of $(C_t(\mathbf{s}), C_t(\mathbf{s}'))$ at each region.

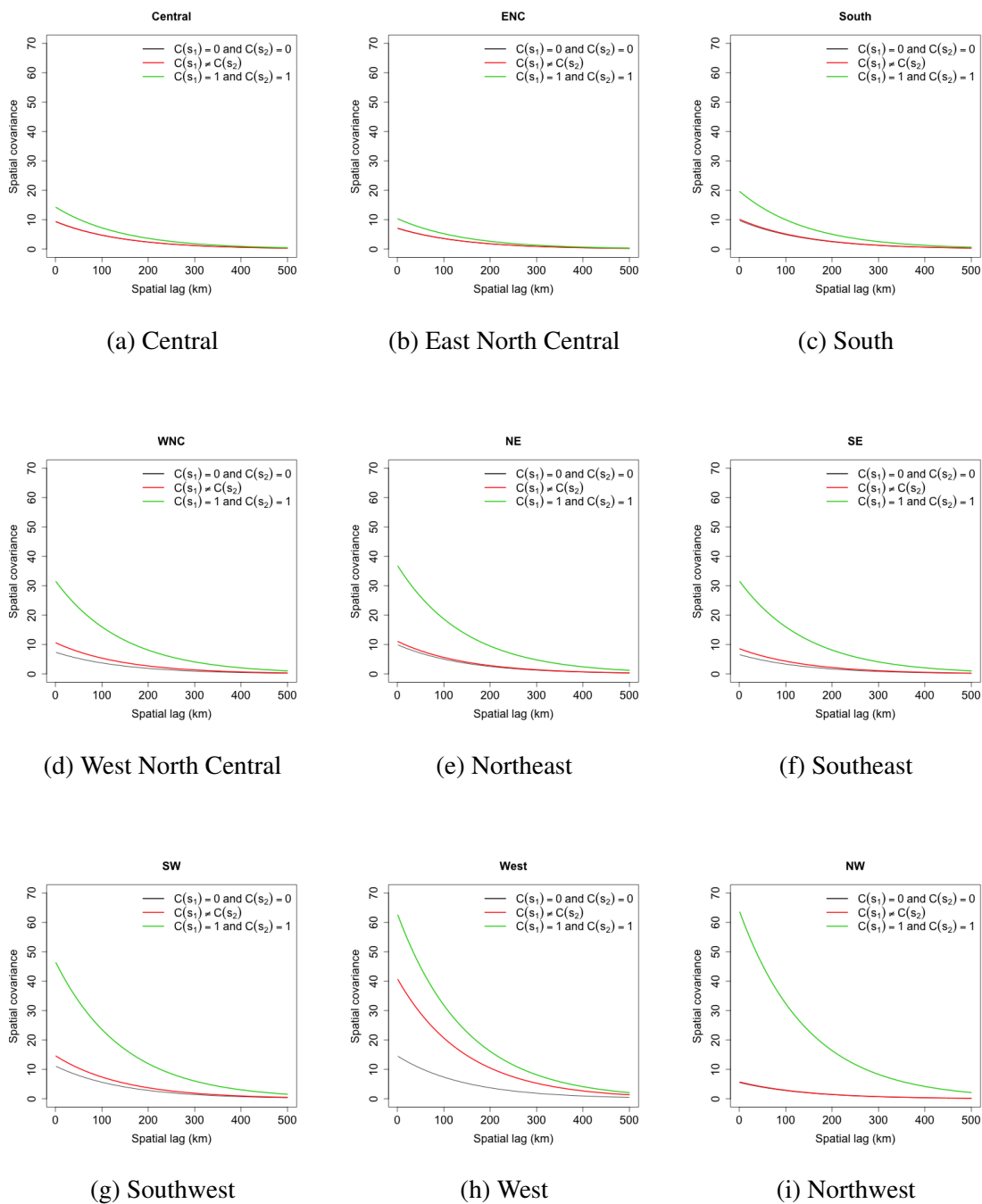
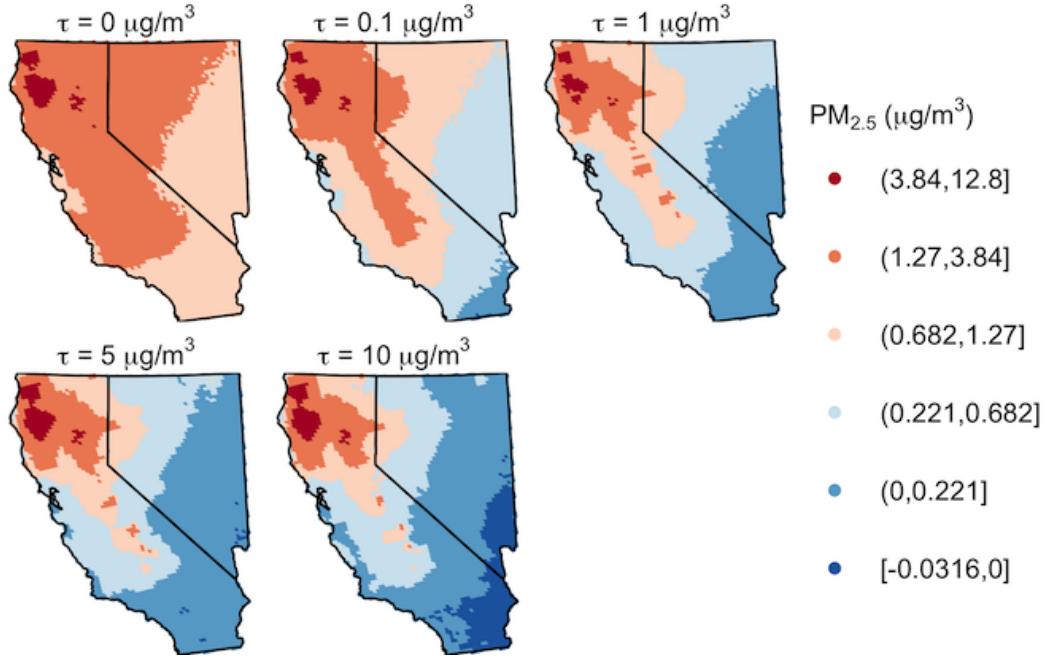


Table 1: **Five-fold cross-validation results for threshold selection, τ ($\mu\text{g}/\text{m}^3$)**, using data from California. We report average (over space and time) mean-squared error (MSE), root mean-squared error (RMSE), mean absolute difference (MAD), standard deviation of the predicted values (SD) and coverage of 95% prediction intervals to assess each model’s ability to predict total $\text{PM}_{2.5}$.

	Threshold, τ ($\mu\text{g}/\text{m}^3$)				
	$\tau = 0$	$\tau = 0.1$	$\tau = 1$	$\tau = 5$	$\tau = 10$
MSE	12.59	12.63	12.58	12.71	12.61
RMSE	3.55	3.55	3.55	3.57	3.55
MAD	1.78	1.77	1.78	1.78	1.77
SD	11.84	11.68	11.58	11.47	11.48
Coverage	0.98	0.98	0.98	0.98	0.98

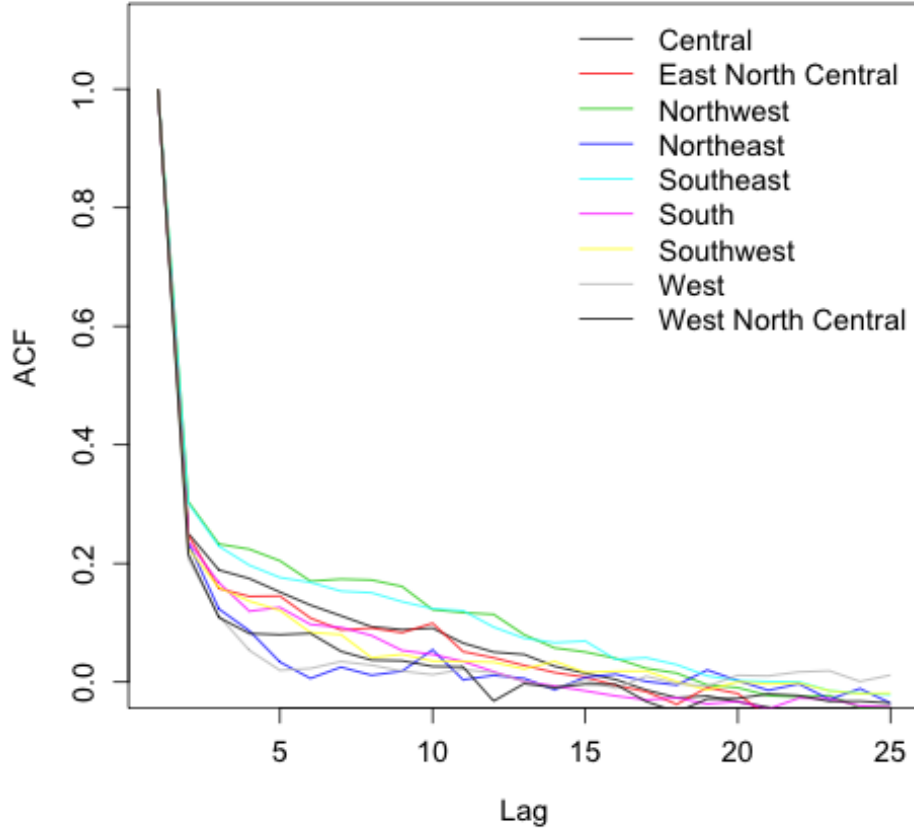
Figure 5: **The causal effect given different smoke thresholds.** The causal effect estimate is robust to the choice of smoke threshold, τ . This is demonstrated in the maps below, which show the causal effect estimate in the Northwest Region for $\tau = 0, 0.1, 1, 5, 10$.



5 Residual Autocorrelation

In this section, we present diagnostics to support our assumption of temporal independence between observations. In Figure 6, we plotted residual autocorrelation functions for each region. The residuals are from the linear regression (separate at each site) of the observations $Y_t(\mathbf{s})$ onto the CMAQ covariates $C_t(\mathbf{s})$, $\hat{\theta}_t(\mathbf{s})$ and $C_t(\mathbf{s})\hat{\delta}_t(\mathbf{s})$. We observe that for all of the regions, the lag-one autocorrelation is around 0.2 for most regions.

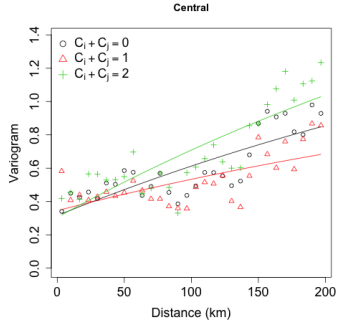
Figure 6: Residual Autocorrelation Function (ACF).



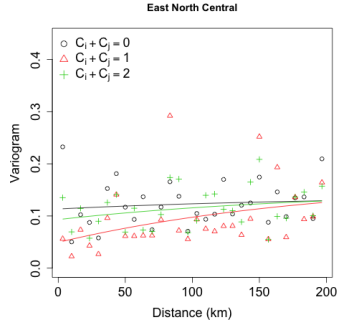
6 Spatial Dependence Model Goodness-of-Fit

We examined variograms of the residuals for each region to determine goodness-of-fit for our spatial dependence model. Figure 7 shows the variograms for all nine regions. We computed the empirical variogram for each combination of $C_t(\mathbf{s})$, shown in different colors, as well as the variogram curves evaluated at the posterior means of the covariance parameters, shown as lines.

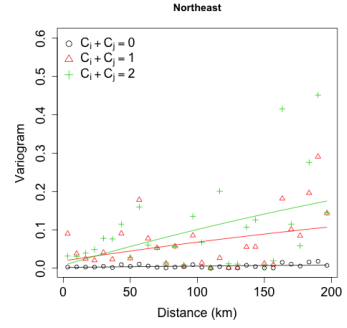
Figure 7: Spatial variograms.



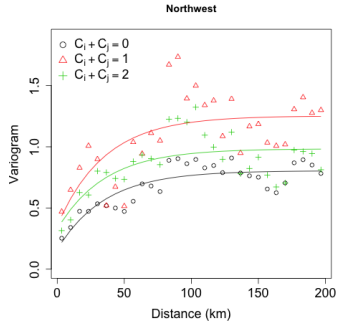
(a) Central



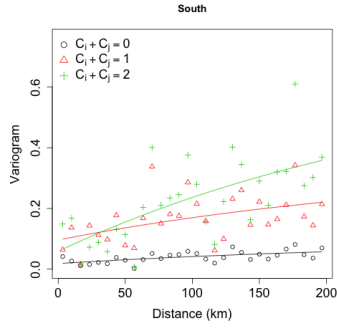
(b) East North Central



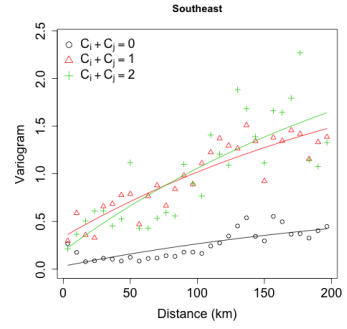
(c) Northeast



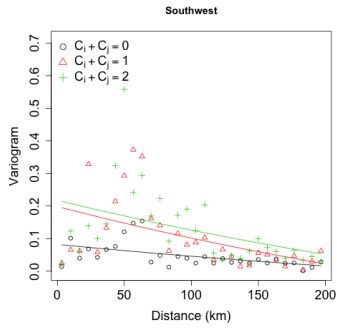
(d) Northwest



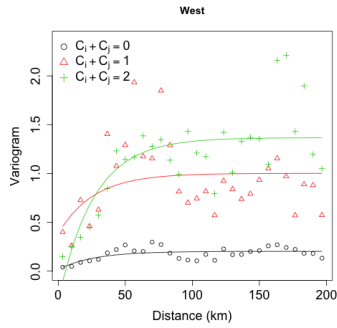
(e) South



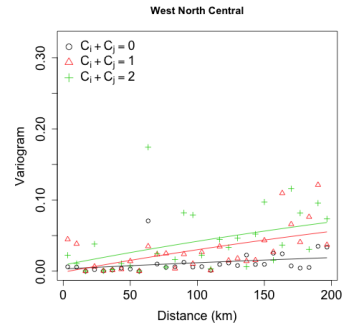
(f) Southeast



(g) Southwest



(h) West



(i) West North Central